Metabolism, transport, and physiologically based pharmacokinetic modelling of novel tacrine derivatives

by

Alanna McEneny

A thesis

presented to the University of Waterloo

in fulfillment of the

thesis requirement for the degree of

Master of Science

in

Pharmacy

Waterloo, Ontario, Canada, 2015

Author's Declaration

I hereby declare that I am the sole author of this thesis. This is a true copy of the thesis, including any final revisions, as accepted by my examiners.

I understand that my thesis may be made electronically available to the public.

Abstract

Alzheimer's disease (AD) is the most prevalent form of dementia affecting the elderly population, and its burden is rapidly growing both in Canada and worldwide. As a result, there is a substantial need for more effective treatments. The first drug that was approved for the management of AD symptoms was tacrine, a dual cholinesterase inhibitor. However, tacrine has since been discontinued after signs of hepatotoxicity were observed in a considerable proportion of patients. This toxicity has been linked to certain metabolites of tacrine formed by oxidation via the hepatic enzyme CYP1A2. Despite this issue, tacrine has remained a popular scaffold for the design of novel anti-Alzheimer's agents. While tacrine is an example of the "one drug, one target" approach, a popular strategy involves functionalizing tacrine into a multi-targeted compound to target several pathways in the complex pathology of AD.

In this regard, a library of tacrine derivatives was developed that exhibited both potent cholinesterase inhibition and the ability to inhibit the formation of the characteristic beta-amyloid plaques. Out of 25 starting compounds, nine compounds were examined further using *in vitro* and *in silico* techniques to investigate binding interactions with CYP1A2 and CYP3A4 (to assess potential for hepatotoxicity) and P-gp (to predict central nervous system permeability). Three of the remaining nine compounds displayed the desired properties and further experiments were conducted with these compounds to determine metabolic clearance. These results were incorporated into a physiologically based pharmacokinetic model that was used to predict the dose needed to reach target brain concentrations in a preclinical study.

Acknowledgements

I would like to thank to the University of Waterloo School of Pharmacy for supporting the work presented here. I also wish to thank the Ontario Graduate Scholarship (OGS), Rx&D Canada, the CIHR Drug Safety and Efficacy Cross-Disciplinary Training program, the Association of Faculties of Pharmacy of Canada and the Graduate Studies Office for their funding of the project and conference expenses.

I wish to thank Anil Maharaj, Rabiya Chandani, Dr. Colin Phipps, and Tarek Mohamed for their support during the project. I would also like to acknowledge Dr. Binbing Ling (University of Guelph) for her expertise, as well as Nancy Gibson (Central Animal Facility) and Dr. Eric Bombardier (Department of Kinesiology) for the use of their facilities. I also wish to thank Drs. Andrea Edginton and Praveen Rao for their support and mentorship throughout this project. Finally, I would also like to extend my appreciation to my committee members, Dr. Marianna Foldvari and Dr. David Rose, for their support and feedback over the past two years.

Dedication

I would like to dedicate the efforts presented here to my husband, Scott King, who has been a constant source of support and encouragement throughout my academic career. This work is also dedicated to my parents, Elgin and Linda McEneny, who have been my greatest cheerleaders and whose good examples have taught me to work hard for the things that I aspire to achieve.

Table of Contents

List of Figures

List of Tables

List of Abbreviations

Aβ – Amyloid beta

ACh – Acetylcholine

AChE – Acetylcholinesterase

AD – Alzheimer's disease

ADP – Adenosine diphosphate

Ala – Alanine

APP – Amyloid precursor protein

Asp – Aspartic acid

ATP – Adenosine triphosphate

Å – Angstrom

B:P – Blood-to-plasma partition coefficient

BBB – Blood-brain barrier

BuChE – Butyrylcholinesterase

CDE – CDOCKER energy

CDIE – CDOCKER interaction energy

ChAT – Choline acetyltransferase

ChEI – Cholinesterase inhibitor

Cl – Chlorine

CL_{int} – Intrinsic clearance

$CL_{int,s}$ – Scaled intrinsic clearance

ClogP – Calculated logP

cm – Centimetre

C_{max} – Maximum concentration

CNS – Central nervous system

C_{ss} – Steady state concentration

CYP1A2 – Cytochrome P450 1A2

CYP3A4 – Cytochrome P450 3A4

CYP450 – Cytochrome P450 enzymes

DMSO – Dimethyl sulfoxide

ΔA_{420} – Change in absorbance at 420 nanometres

EC_{50} – Half maximal effective concentration

EDTA – Ethylene diamine tetraacetic acid

ε – Extinction coefficient

FDA – US Food and Drug Administration

f_u – Fraction unbound

g/mol – Grams per mole

GBSW – Generalized born with a simple switching

GFR – Glomerular filtration rate

Gln – Glutamine

Gly – Glycine

IC_{50} – Concentration required to inhibit 50% of activity

IC_{90} – Concentration required to inhibit 90% of activity

Ile – Isoleucine

IV – Intravenous

IVIVE – *In vitro-in vivo* extrapolation

kcal/mol – Kilocalories per mole

KCl – Potassium chloride

k_{dep} – Depletion rate constant

K_m – Michaelis-Menten constant

K_p – Partition coefficient

Leu – Leucine

logP – Octanol-water partition coefficient

ℓ - Path length

M – Moles per litre

MeOH – Methanol

Met – Methionine

mg – Milligram

mL – Millilitre

mM – Millimolar

MW – Molecular weight

$NADP^+$ (NADPH) – Nicotinamide adenine dinucleotide phosphate (reduced form)

NBD – Nucleotide-binding domain

nm – Nanometer

OCT – Organic cation transporter

P-gp – P-glycoprotein

PAS – Peripheral anionic site

PBPK – Physiologically based pharmacokinetic

PDB – Protein data bank

Phe – Phenylalanine

PK – Pharmacokinetics

pK_a – Negative logarithm of the acid dissociation constant

PMSF – Phenylmethylsulfonyl fluoride

R^2 – Coefficient of determination

RFU – Relative fluorescence unit

RLU – Relative luminescence unit

rpm – Rotations per minute

SD – Standard deviation

Ser – Serine

SF – Scaling factor

Thr – Threonine

TMD – Transmembrane domain

tris – Tris(hydroxymethyl)aminomethane

Trp – Tryptophan

Tyr – Tyrosine

µL – Microliter

µM – Micromolar

Val – Valine

w/v – Weight per volume

WHO – World Health Organization

YLD – Years lived with disability

Chapter 1.0 Introduction

1.1 History and Impact of Alzheimer's Disease

Alzheimer's disease (AD) is a progressive neurodegenerative disorder, and is currently the most common cause of cognitive dysfunction in the elderly population. It was identified in 1906 by Alois Alzheimer, who first described the symptoms and neuropathological traits of the disease that would later bear his name.[1] In the United States, 5.3 million people suffer from AD and the costs associated with AD and related dementias will total $226 billion in 2015[2]; a Canadian study conducted in 2011 estimated that 747,000 Canadians live with cognitive impairment, with associated costs of $33 billion per year.[3] These figures are quickly increasing, as the fastest growing age demographic in Canada and the United States continues to be those 85 years and older. Considering that the risk of developing AD doubles every five years after age 65, the prevalence and economic liability of AD are predicted to quadruple by 2050.[4]

1.2 The Cholinergic Hypothesis

Despite the tremendous social and economic burdens of this disease, the compounds available for the treatment of AD only offer symptomatic relief and are unable to alter the course of the disease. A major obstacle in the development of effective AD treatments is its complex pathogenesis. No single cause has been identified; rather, a number of inter-related hypotheses have been proposed. The idea that has inspired almost all existing anti-Alzheimer's agents is the cholinergic hypothesis, which suggests that the symptoms of AD can be attributed to decreased activity of the enzyme choline acetyltransferase (ChAT) in the cortex and hippocampus. ChAT synthesizes the

neurotransmitter acetylcholine (ACh) from the compounds acetyl-CoA and choline (Figure 1), and a correlation between loss of ChAT activity and formation of neurofibrillary tangles and senile plaques (two anatomical hallmarks of AD) was first noted in the 1970s.[5] Anatomical studies have indicated that the cortex is not uniformly affected, and suggest that the disease begins in the hippocampus, followed by the temporal, frontal and parietal lobes.[6] This proposed pathology aligns well with clinical observations, as the earliest and most prominent symptom of AD is loss of memory, a function in which the hippocampus has a substantial role.[7] The idea that the pathogenesis of Alzheimer's disease was related to the degradation of a specific cell population led to the hope that cholinergic replacement would be as successful as dopamine replacement in the treatment of Parkinson's disease. Several metabolic precursors[8,9] and cholinergic agonists[10] reached clinical trials, but were unsuccessful in improving disease state.[11]

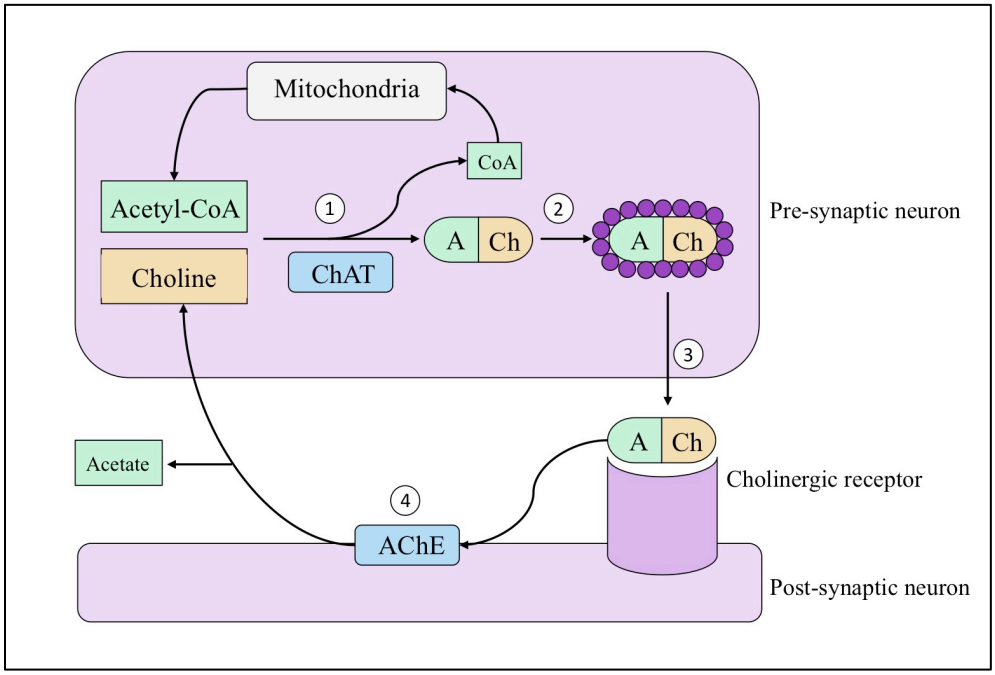

Figure 1. Synthesis and degradation of acetylcholine. (1) ACh is synthesized from the precursors acetyl-CoA and choline by ChAT. (2) ACh is stored in vesicles, which then undergo fission (3) to release ACh so that it may bind to receptors. (4) After dissociating from the receptor, ACh is hydrolyzed by AChE into acetate and choline, which is recycled into the pre-synaptic neuron to produce more ACh.

1.2.1 Cholinesterase Inhibitors

As a result, new strategies were developed to increase ACh levels in the brain. ACh is regularly hydrolyzed by acid catalysis through the cholinesterase enzymes, acetylcholinesterase (AChE) and butyrylcholinesterase (BuChE).[12] Under normal physiological conditions, AChE is primarily responsible for the degradation of ACh, but BuChE levels rise in late-stage AD patients such that BuChE becomes the primary catalyst for ACh hydrolysis.[13] It was hypothesized that the inhibition of these enzymes

could maintain ACh levels. Today, cholinesterase inhibitors (ChEIs) represent the major class of compounds used in the pharmacotherapy of AD; among the four drugs approved in Canada for the management of AD symptoms, three are ChEIs (Figure 2).[14] These agents include donepezil (Aricept®), galantamine (Reminyl®) and rivastigmine (Exelon®); the fourth option, memantine (Namenda®), is an *N*-methyl-D-aspartate receptor antagonist and can be used alone or in combination with donepezil in severe cases of AD.[15] However, these compounds only treat the symptoms of mild to moderate AD rather than stopping or reversing the disease progression, indicating a need to target multiple pathways to find more effective therapies.

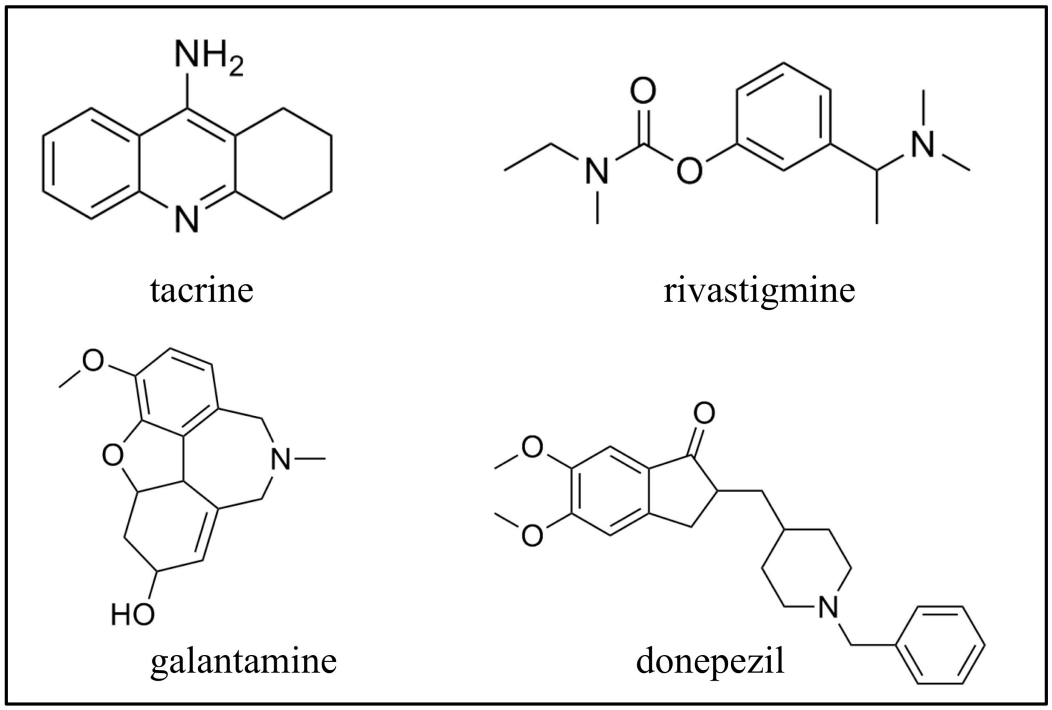

Figure 2. Chemical structure of existing cholinesterase inhibitors used in the treatment of Alzheimer's disease.

1.3 The Amyloid Cascade Hypothesis

In the early 1990s, a new hypothesis emerged that suggested that the amyloid-β protein (Aβ) that forms the characteristic plaques observed in AD brain is actually a principal driver of AD pathology rather than a marker of the disease.[16] Aβ peptide is produced by the proteolysis of the much larger, membrane-associated amyloid precursor protein (APP). The processing of APP can follow one of two pathways: amyloidogenic or non-amyloidogenic. In the non-amyloidogenic pathway, APP is cleaved within the Aβ domain of the protein by α-secretase, preventing the formation of Aβ protein. Alternatively, APP may be cleaved by β-secretase near the N-terminus of the Aβ region and by γ-secretase near the C-terminus, thus releasing Aβ protein (Figure 3). The C-termini of these proteins contain several hydrophobic residues that allow the peptide to aggregate into dimers, oligomers and fibrils.[17] Although it has been shown to consist of anywhere between 39 and 43 amino acid residues, the two primary forms are the species comprised of 40 and 42 amino acid ($A\beta_{40}$ and $A\beta_{42}$, respectively). Although $A\beta_{42}$ only accounts for ~10% of total secreted Aβ, it is the most toxic form of amyloid aggregates.[18] These amyloid species modify the electrical activity of surrounding neurons, thus causing neuronal dysfunction.[19]

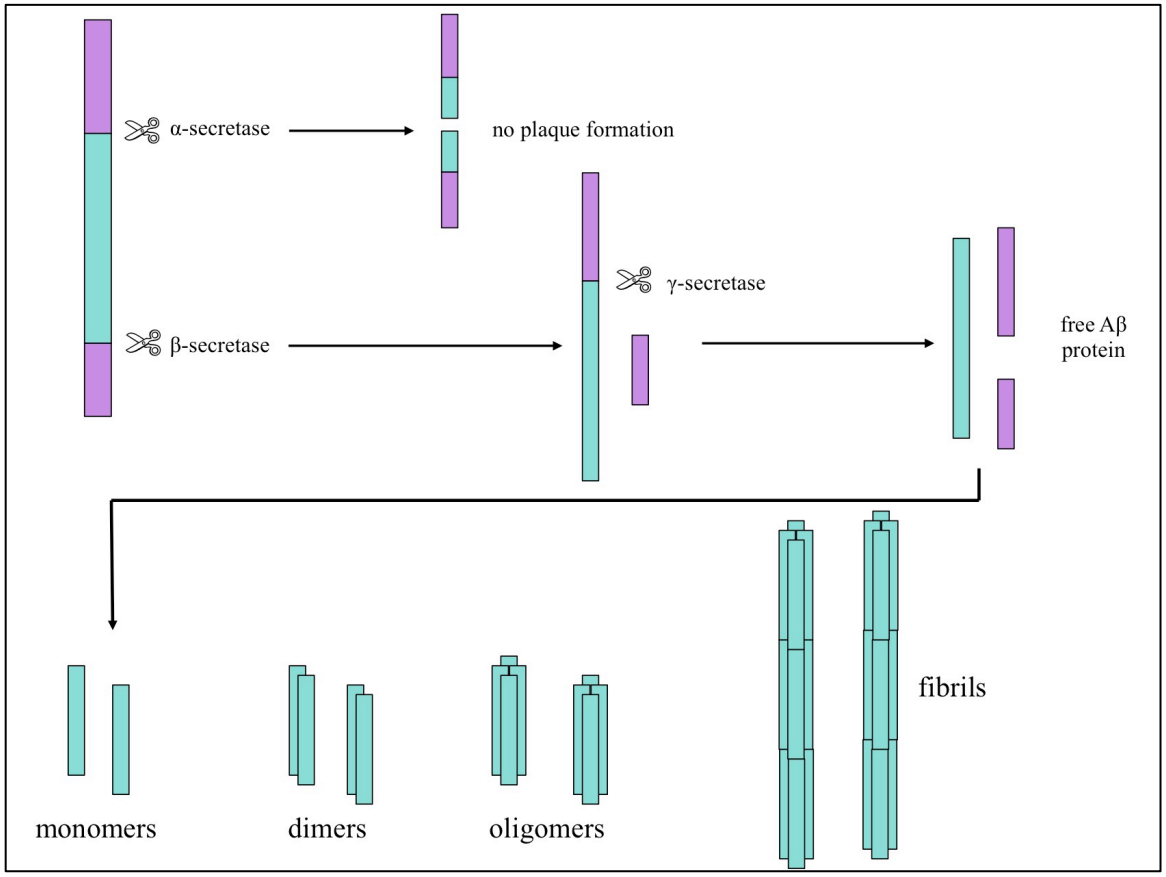

Figure 3. Release of Aβ protein following cleavage by β- and γ-secretase, and subsequent aggregation into dimers, oligomers and fibrils.

1.3.1 AChE-Induced Amyloid Aggregation

Shortly after its introduction, a concrete link between the amyloid cascade and cholinergic hypotheses was identified. AChE, the enzyme primarily responsible for ACh degradation, was found to co-localize with Aβ deposits, forming a neurotoxic complex at the peripheral anionic site (PAS) of the enzyme.[20] The PAS is composed of five residues (Tyr70, Asp72, Tyr121, Trp279 and Tyr334) and serves to guide ACh into the catalytic site, which is found at the bottom of a 20 Å gorge.[21] In AChE-promoted amyloid

aggregation, it is proposed that the PAS acts as a nucleation centre to accelerate the assembly of Aβ fibrils, which is consistent with the observation of AChE within the senile plaques in AD brains. Furthermore, Aβ-AChE complexes have been shown to be more toxic than Aβ fibrils alone. An *in vivo* study in rat hippocampus showed larger amyloid deposits, extensive astrocytosis and greater neuronal cell death in animals injected with Aβ-AChE complexes compared to Aβ injections alone.[22]

1.4 Tacrine

Tacrine (Cognex®) was the first compound to be approved by the US Food and Drug Administration (FDA) for the management of AD symptoms. It is a potent inhibitor of both AChE and BuChE, binding primarily in the catalytic site.[23] However, tacrine has since been removed from the market due to adverse effects, including hepatotoxicity in a significant percentage of patients.[24] This toxicity has been attributed to certain metabolites produced when tacrine undergoes oxidative hydroxylation by the hepatic enzyme cytochrome P450 1A2 (CYP1A2). This addition can occur at the C-1, C-2, C-4 and C-7 positions, and subsequent rearrangement to a reactive 7-quinone methide intermediate can occur (Figure 4). This species is able to bind irreversibly to surrounding macromolecules, causing hepatocellular necrosis.[25] This mechanism is similar to that of acetaminophen, which also produces a quinone-based metabolite causing liver toxicity.[26]

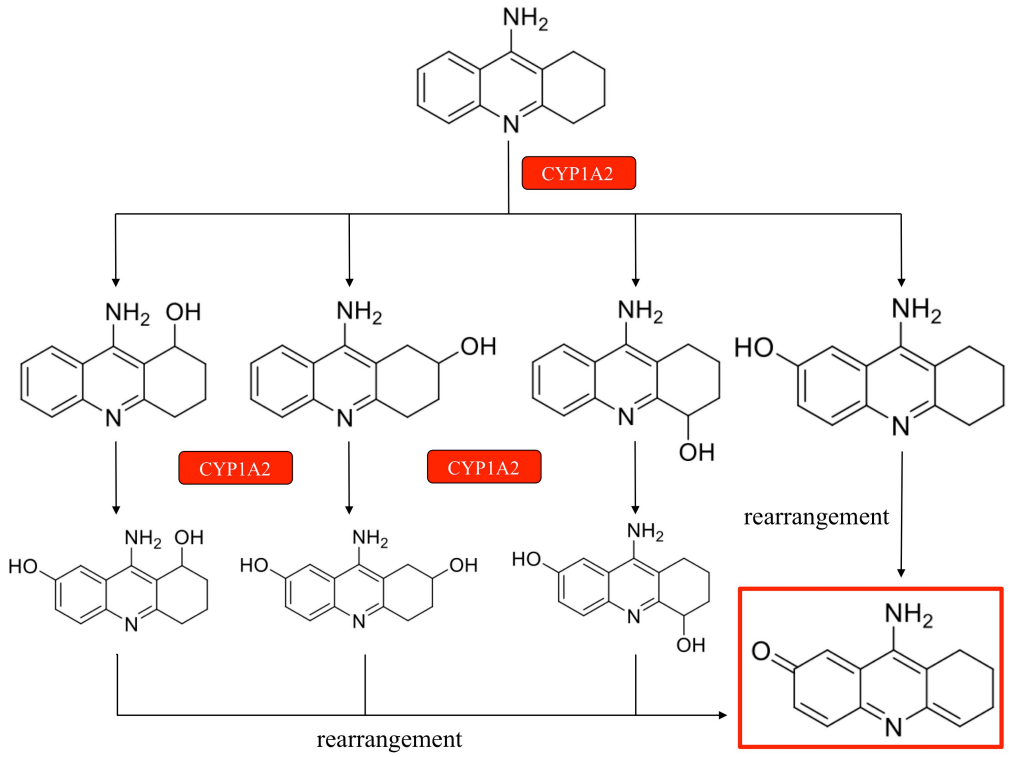

Figure 4. Metabolic profile of tacrine illustrating the formation of a reactive quinone methide species (red box) via metabolism of CYP1A2

1.4.1 CYP1A2

The cytochrome P450 family of enzymes catalyze the oxidative metabolism of a wide variety of xenobiotics, including approximately 75% of total drug metabolism.[27] Although CYP3A4 catalyzes the majority of these reactions, a growing focus has been placed on the CYP1A2 isozyme due to its potentially clinically relevant role in an increasing number of compounds.[28] Most CYP1A2 substrates, including tacrine, can be categorized as polycyclic aromatic hydrocarbons; high lipophilicity, neutral or basic behaviour, low molecular volume (< 200 $Å^3$) and the presence of at least one hydrogen

bond donor are also common traits among CYP1A2 substrates.[29] The small size and planar nature of most CYP1A2 substrates is due to its relatively narrow active site (375 $Å^3$) compared to other CYPs (e.g. 1385 $Å^3$ for CYP3A4).[30] The substrate-binding site is enclosed by the Phe226 residue on Helix F and the Gly316-Ala317 peptide on Helix I, which form two parallel platforms on either side of the binding cavity. Each of these helices also contains a polar residue (Thr223 on Helix F; Asp320 on Helix I) that undergoes strong hydrogen bonding interactions to stabilize the shape of the active site. Several polar amino acids can also be found near the entrance to the CYP1A2 active site (Thr118, Ser122 and Thr124) that are unique to this CYP450 isozyme and are thought to contribute to substrate positioning through hydrogen bonds (Figure 5).[31] Furthermore, studies using the random mutagenesis approach have shown that CYP1A2 catalytic activity is substantially reduced when mutations occur at the Phe226 and Asp320 residues, providing further evidence of the major roles these amino acids play in substrate binding.[32]

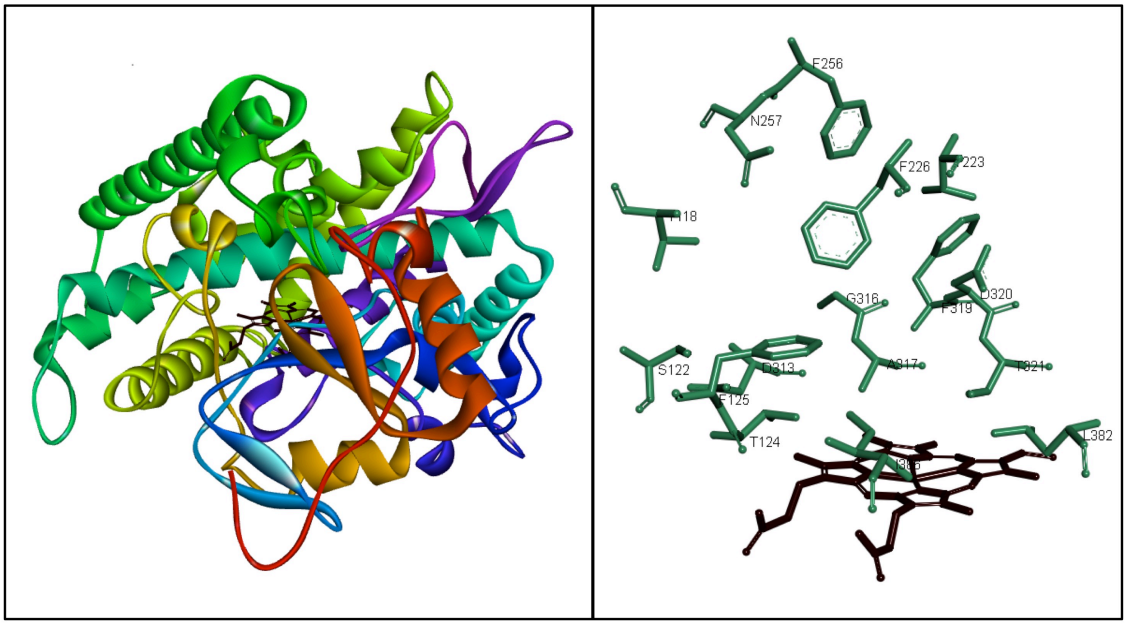

Figure 5. Left: 3D structure of CYP1A2 (PDB file name: 2HI4). Right: The CYP1A2 active site. *Dark red:* heme prosthetic group; *green:* key amino acids.

1.4.2 Tacrine-Based Derivatives as Potential Anti-Alzheimer's Agents

Despite this issue of toxicity, tacrine remains a popular framework for the design of novel anti-Alzheimer's agents with the ability to target multiple factors associated in AD pathophysiology. Typically, an analogue will feature a new functional group at the C-9 amine of tacrine to combine its inhibitory activity toward cholinesterases with another therapeutic action. These added functional groups may contribute to antioxidant activity,[33] vascular relaxation,[34] anti-amyloid aggregation,[35] or NMDA reception modulation.[36] In addition to targeting multiple pathways in AD pathology, these derivatives are designed with the intent of reducing the adverse effects observed with tacrine, with particular emphasis on hepatotoxicity. In this regard, Wesseem Osman, a former graduate student in Dr. Nekkar Rao's lab at the University of Waterloo, developed

a library of novel tacrine derivatives (Figure 6).[37] These compounds incorporate moieties from curcumin and resveratrol, which are known antioxidants and are involved in the degradation of Aβ oligomers.[38,39] The novel tacrine derivatives prepared by Osman act as dual inhibitors of both cholinesterase enzymes with anti-amyloid aggregation properties. They exhibit potent cholinesterase inhibition, with half maximal inhibitory concentration (IC_{50}) in the nanomolar to micromolar range. Additionally, selected compounds have been shown *in vitro* to inhibit self-induced amyloid aggregation of $A\beta_{40}$ (65.8-97.1% at 25 μM) and $A\beta_{42}$ (49.4-81.4% at 25 μM) in *in vitro* experiments, which is significantly greater than the inhibition observed for tacrine (7% at 100 μM), donepezil (22% at 100 μM),[40] and galantamine (~40% at 50 μM).[41] These compounds are also predicted to inhibit AChE-induced amyloid aggregation through interaction at the peripheral anionic site of AChE, based on *in silico* molecular docking experiments. Although these derivatives displayed potent activity towards multiple AD pathways, it was still unknown whether these derivatives would also form hepatotoxic metabolites *in vivo* due to their structural similarity to tacrine. We addressed this by investigating the binding affinity and orientation of these novel tacrine derivatives within CYP1A2 *in silico* and by performing *in vitro* metabolism experiments to identify metabolites and evaluate clearance.

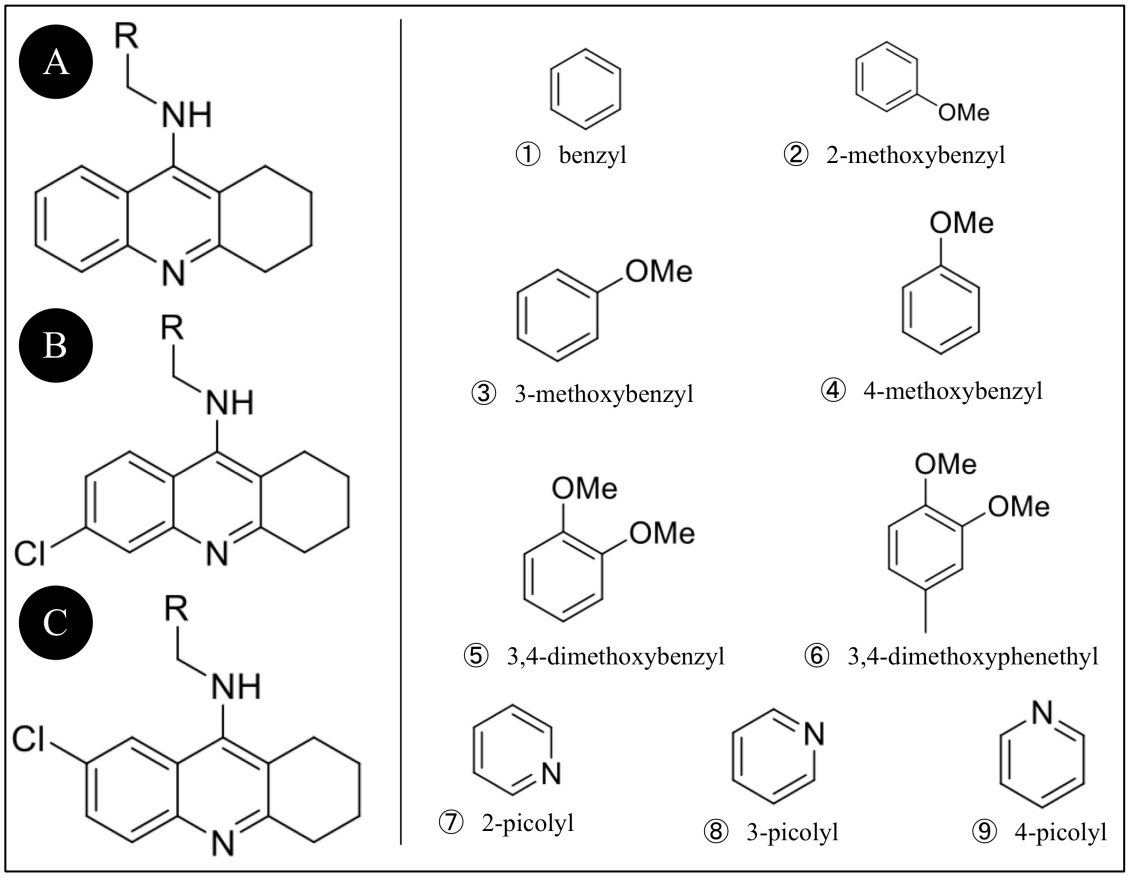

Figure 6. Chemical structures of novel tacrine derivatives. Compounds are named by combining the letter for their class and the number for the appropriate substituent. For example, B2 is **6-chloro**-*N*-(**2-methoxybenzyl**)-tacrine.

1.5 Development of CNS-Targeted Drugs

Despite a relatively high prevalence, neurological and psychiatric disorders apply a disproportionately large burden on global health systems. One way of quantifying the burden of a chronic disease is in terms of years lived with disability (YLD). In 2000, the World Health Organization (WHO) estimated that neuropsychiatric disorders accounted for 31% of YLDs worldwide; in developed countries, where infectious diseases and

malnutrition are less prevalent, over 40% of YLDs can be attributed to neurodegenerative and psychiatric diseases.[42] This tremendously high burden emphasizes the urgent need for more effective agents against these diseases.

However, several large pharmaceutical companies have recently shut down the neurological disorders cohorts of their research and development operations. The search for new treatments for this group of diseases has become too costly, with the risk of failure outweighing the potential rewards. Agents targeting the central nervous system (CNS) are much more difficult to develop than other types of drugs, with only 8.2% of drug candidates reaching the market compared to 15% of drugs overall. These failings also tend to occur in later stages of the drug development process, making their development even more resource-intensive. Fewer than half of all CNS candidates that reach Phase III trials succeed, compared to a 66% success rate for all other drugs.[43] This high attrition rate can be due to a number of factors including a lack of predictive animal models, an inability to foresee who will benefit from the treatment and the use of subjective diagnostic scales to measure outcomes, where fluctuations in a patient's conditions can make it difficult to evaluate cognitive improvement.[44] Their long-term use also necessitates more testing for safety and efficacy compared to a treatment that lasts only a few days. As a result, human testing of CNS agents typically lasts two years longer than average drug candidates.

1.5.1 Lipophilicity and Other Factors Influencing CNS Permeability

Considering the hurdles that must be overcome to develop a new CNS-targeted therapy, it is crucial that only the most promising candidates are moved forward and that key properties be investigated early in the drug development process. In addition to high potency and selectivity for the target, there are a number of other characteristics that promote successful CNS activity. The first property to be linked to CNS activity was the octanol-water partition coefficient, logP, which is a measure of lipophilicity. Although logP has an experimental origin and interpretation, it is now more common to determine the calculated logP (ClogP), which can be estimated by a number of different algorithms based on the aromatic rings and functional groups contained in the compound. This dependence was first reported by Hansch and coworkers in 1967, who found that this relationship was parabolic in nature rather than linear.[45] Although high lipophilicity does facilitate CNS penetration, this parameter can be described as a "double-edged sword." The compound must be lipophilic enough to penetrate the brain, but not so lipophilic that its solubility, absorption and metabolic stability are compromised.[46] Increased lipophilicity is also associated with a greater likelihood of promiscuous receptor binding, resulting in toxicity – a well-documented phenomenon for anaesthetics.[47,48] Despite the negative influence of high lipophilicity on a compound's pharmacokinetics (PK) and toxicity profile, a current trend in drug discovery is a focus on candidates with high molecular weight and high logP values, driven by the enhanced potency of lipophilic molecules. This inclination towards achieving potency by increasing size and lipophilicity has been termed "molecular obesity," and has been implicated in high attrition rates during drug development.[49]

A number of other physicochemical properties, some of which are related to lipophilicity, have been linked to the success or failure of CNS-targeted drugs. Lipinski, known for his Rule of Five describing favourable properties for orally active drugs,[50] developed a more stringent set of criteria for predicting CNS penetration. These include lower molecular weight (≤400 g/mol) and fewer hydrogen bond donors and acceptors (≤3 and ≤7, respectively).[51] Sufficient aqueous solubility is crucial, as passive diffusion into the brain is driven by the concentration gradient between blood and brain. Molecular flexibility, expressed as the number of rotatable bonds in the structure, also plays a role in CNS penetration. Increased molecular flexibility impedes the molecule's ability to traverse membranes, so a more rigid structure (fewer than 7 rotatable bonds) is desirable.[52]

1.5.2 P-glycoprotein

As mentioned, lipophilicity is a key factor in determining the ability of a compound to penetrate the CNS but does not guarantee entry into the brain. The blood-brain barrier (BBB), a highly selective barricade of tightly joined endothelial cells, protects the brain from neurotoxins and extracellular fluctuations in hormones or amino acids that can lead to uncontrolled brain activity.[53] Although highly lipophilic compounds are able to infiltrate the physical component of the BBB, their entrance into the CNS may be modulated by the transporter P-glycoprotein (P-gp). Transport by P-gp poses a significant challenge to pharmacologists due to its remarkably extensive poly-specificity, binding compounds with a wide range of lipophilicities and molecular weights.[54] Structurally, P-gp consists of two analogous halves, each containing six transmembrane domains (TMDs) and a nucleotide-binding domain (NBD). A funnel-shaped internal cavity (6000 $Å^3$) is contained within the TMDs and features a flexible binding pocket with hydrophilic groups, charged groups and aromatic amino acids to accommodate a wide variety of substrates (Figure 7).[55]

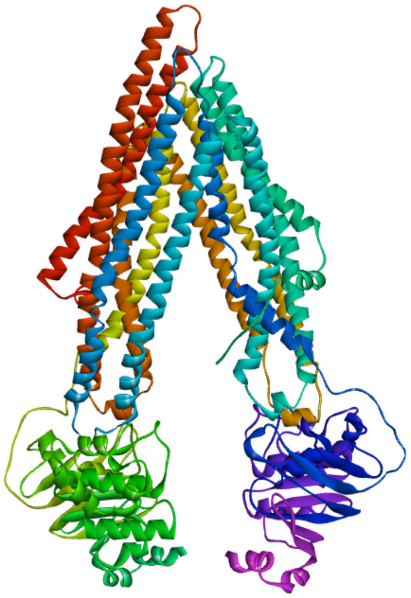

Figure 7. 3D structure of murine P-gp (PDB file name: 3G61) in the inward-facing conformation.

At the start of the catalytic cycle, P-gp is in its inward-facing conformation and the compound binds to one of the high affinity sites found within the TMDs, entering from either the inner leaflet of the membrane or from the cytoplasmic side of the protein. The binding of the drug increases the affinity of P-gp for ATP and induces a conformational change in which the NBDs dimerize while each is bound to a molecule of ATP; this is called the outward-facing conformation. This change in conformation reduces the activation energy and moves the drug to a lower affinity site, from which it is released following the hydrolysis of ATP. The second molecule of ATP is hydrolyzed and the energy provided is used to separate the NBD dimer, resetting the protein to its initial state (Figure 8).[56,57] An alternate model for this transport cycle has been suggested, which also requires the hydrolysis of two molecules of ATP. However, this model

proposes that only one molecule of ATP is bound at any given time, with the first ATP hydrolysis powering the efflux of the drug and the second serving to return P-gp to its ground state

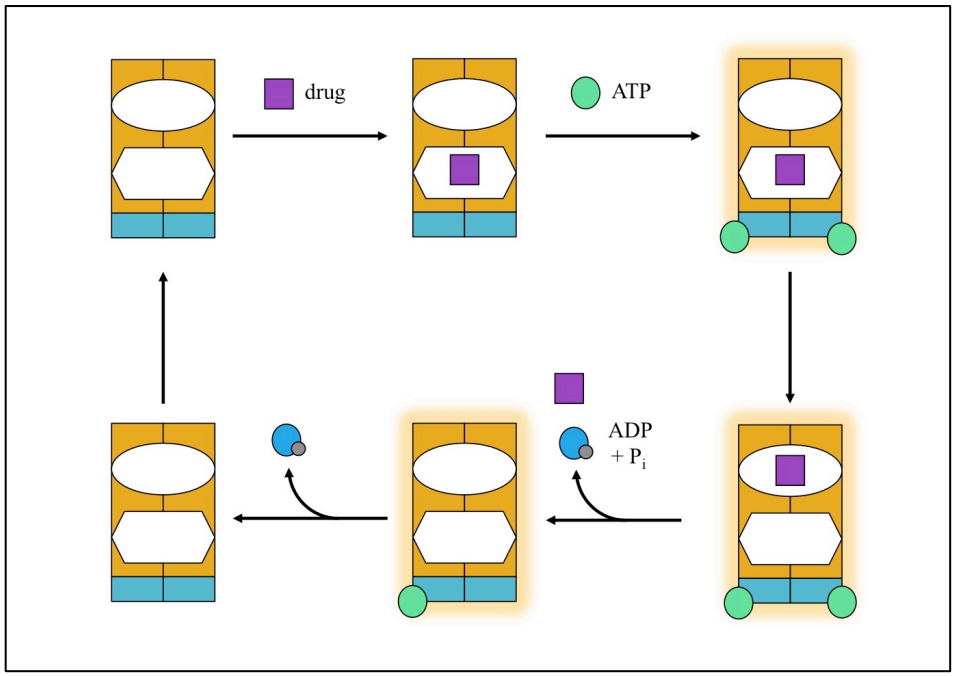

Figure 8. The P-gp catalytic cycle: Drug binds to a high affinity site (hexagon) within the TMDs. One molecule of ATP binds to each of the NBDs, causing them to dimerize and moving the drug to a low affinity site (oval). Hydrolysis of one molecule ATP to ADP and P_i powers the release of the drug. The second molecule of ATP is hydrolyzed to separate the NBD dimer, resetting P-gp to its initial, inward-facing conformation.

A drug's relationship with P-gp, whether it is a substrate, inhibitor or inducer, can have many clinically significant implications. If a CNS-targeted drug undergoes transport by P-gp, it can be difficult to reach the concentration needed to observe a therapeutic effect. For other orally administered drugs, P-gp can also present a challenge. P-gp is

expressed in the apical intestinal membrane, where liver enzymes including CYP3A4 are also found. There is known to be considerable overlap in the substrate specificities of P-gp and CYP3A4, so repeated transport by P-gp across the intestinal membrane provides greater opportunity for intestinal metabolism to occur, resulting in low oral bioavailability.[58] As a result, oral absorption and CNS penetration can be improved by concomitant use of P-gp inhibitors, which has been demonstrated with the anticancer drug paclitaxel.[59] However, the simultaneous use of P-gp substrates and inhibitors can also result in adverse effects. For example, colchicine is a CYP3A4 and P-gp substrate that, when taken with an inhibitor of these enzymes, can be lethal; more than 60 deaths have been linked to the co-administration of colchicine and the antibiotic clarithromycin, a strong inhibitor of CYP3A4 and P-gp.[60] For these reasons, it is very important to determine how a drug candidate interacts with P-gp.

1.6 Physiologically Based Pharmacokinetic Modelling in Drug Development

Physiologically based pharmacokinetic (PBPK) modelling is an *in silico* technique that can be employed in numerous stages of drug discovery and development, including first-in-human trials, drug-drug interaction studies and candidate selection.[61] These models incorporate both the properties of the compound of interest (such as molecular weight, ClogP, acid-base behaviour, fraction unbound and tissue-plasma partition coefficients) and the anatomical and physiological characteristics of the organism (such as blood flows, organ volumes, and tissue compositions). Each compartment within the model represents a specific organ, and the compartments are interconnected via the circulatory system. The drug transfer across all compartments is

expressed as a series of mass balance differential equations, and the amount of drug in any compartment can be calculated for any given time.[62] Because they are mechanistic in nature, these models can be used to extrapolate between species, maturational stages and disease states, offering a distinct advantage over empirically derived pharmacokinetic models where the compartments have little biological relevance. Their mechanistic nature also permits explicit definition of important processes that affect compound disposition such as transporter and metabolic activity.

The ability to predict CNS permeability and brain concentrations is one of the major difficulties in developing CNS-targeted drugs, and is an area where PBPK models can be useful. A number of PBPK models of the CNS have been reported,[63-65] with varying degrees of detail, but an emphasis has recently been placed on the use of an *in vitro-in vivo* extrapolation (IVIVE) strategy. This approach uses scaling factors to transform *in vitro* data, such as clearance, transport activity and permeability, to account for differences between the *in vitro* and *in vivo* environments.[66] Through integration of this data within a PBPK model framework, disposition of the compound in any organ (e.g. brain) can be predicted in a biologically rational manner.

Chapter 2.0 Objectives and Hypotheses

Overall Objective: To identify the most promising candidates from a library of tacrine derivatives for further development by investigating their risk for hepatotoxicity, CNS permeability and metabolic stability

Objective 1: To evaluate tacrine and its derivatives (Figure 6) as potential substrates of CYP1A2

- Aim 1: Conduct *in vitro* CYP1A2 assays and calculate IC_{50} values
    - Hypothesis: Chemical modification of tacrine will alter its binding to CYP1A2. As a result, these derivatives will have different substrate profiles as compared to tacrine.
- Aim 2: Conduct *in silico* molecular modelling experiments to determine binding modes and energy of the ligand-enzyme complexes
    - Hypothesis: The larger molecular volumes of the tacrine derivatives will limit their ability to fit within the narrow CYP1A2 binding site.
- Aim 3: Correlate the results of the *in vitro* and *in silico* experiments to determine the utility of *in silico* models for predicting substrate behaviour
    - Hypothesis: A correlation between IC_{50} and energy parameters for the complex will emerge, linking structural modifications and CYP1A2 substrate behaviour

Objective 2: To evaluate tacrine and its derivatives as potential substrates towards P-gp

- Aim 1: Establish clinically relevant P-gp activity by measuring *in vitro* IC_{50} values and comparing donepezil, a current AD therapy whose behaviour towards P-gp is not well-defined, with ketoconazole, a known P-gp inhibitor
    - Hypothesis: By comparing the binding interactions and ligand-enzyme complex energy of donepezil within P-gp to those of ketoconazole, the role of P-gp in donepezil's disposition can be clarified and serve as a reference for clinically relevant P-gp activity.
- Aim 2: Complete analogous *in silico* and *in vitro* experiments with tacrine, and derivatives and compare with reference compounds ketoconazole and donepezil
    - Hypothesis: It has been reported that the tacrine is not a substrate for P-gp. However, it is possible that the addition of large substituents at the C-9 position will result in enhanced P-gp binding.
- Aim 3: Correlate the results of the *in vitro* and *in silico* experiments to determine the utility of *in silico* models for prediction of substrate behaviour
    - Hypothesis: The combination of *in vitro* and *in silico* data will allow us to more confidently predict P-gp substrate behaviour.

Objective 3: To assess the metabolic profile of the tacrine derivatives

- Aim 1: Isolate rat liver microsomes and quantify their protein content and CYP450 reductase activity
- Aim 2: Calculate *in vitro* intrinsic clearance using a substrate depletion approach
    - Hypothesis: It is expected that the tacrine derivatives will be more metabolically stable (i.e. will have a lower intrinsic clearance) than tacrine.

Objective 4: To develop PBPK models for tacrine and its derivatives

- Aim 1: Parameterize a PBPK model for tacrine in rats following intravenous (IV) administration and compare to observed data for the purpose of optimizing lipophilicity, intrinsic clearance and transport activity
- Aim 2: Determine scaling factors to convert *in vitro* metabolism and distribution parameters from those parameters optimized in the tacrine model
- Aim 3: Develop PBPK models for tacrine derivatives using the same scaling factors and derivative-specific *in vitro* data
- Aim 4: Use the models to predict the IV dose required to reach appropriate brain concentrations

Chapter 3.0 Methods

3.1 Initial Compound Selection

As mentioned, there are a number of physicochemical properties that are useful in predicting the success or failure of a CNS-targeted drug. First and foremost, the compound must be able to achieve therapeutic levels in the target organ. For the tacrine derivatives, target affinity was measured as the half maximal inhibitory concentration (IC_{50}) towards AChE or BuChE. Since AChE is the primary catalyst for acetylcholine hydrolysis, potency towards this enzyme exhibited by tacrine derivatives was analyzed. Among the cholinesterase inhibitors currently available, rivastigmine (Exelon®) has the highest AChE inhibitory potency (IC_{50} = 4.15 ± 0.16 μM[67]) and so only tacrine derivatives that exhibited better potency than rivastigmine were moved forward.

Lipophilicity has also been highlighted as a key predictor of a compound's PK profile. Highly lipophilic compounds tend to have poor solubility, low absorption, metabolic instability and greater risk of toxicity, while hydrophilic molecules are more likely to have difficulties permeating the blood-brain barrier. Noting that the ClogP values for the tacrine library used in this project ranges from 4.02 to 6.64, a lower boundary was not required. In Lipinski's modified Rule of Five for CNS-target compounds, a logP < 5 is desirable. Based on AChE inhibition profile, we considered an upper limit of 6 for ClogP values for tacrine derivatives. High potential for hydrogen bonding (i.e. >7 nitrogen or oxygen atoms or >3 N*H* or O*H* groups) did not result in the exclusion of any compounds.

3.2 Molecular Modelling Studies

This project made use of the Discovery Studio 4.0 Structure-Based Design software from BIOVIA/Accelrys Inc. (San Diego, USA) to investigate compound-enzyme interactions with both CYP450 enzymes and the transporter P-gp. The tacrine derivatives were constructed using the *Build Fragment* module and their geometries were optimized by 500 steps of steepest descent, followed by conjugate gradient minimization (0.1 kcal/mol). These experiments utilized the Chemistry at Harvard Macromolecular Mechanics (CHARMm) force field and the implicit solvent function Generalized Born with a simple Switching (GBSW). The crystal structures of CYP1A2, CYP3A4 and P-gp were obtained from the protein data bank (2HI4.pdb, 2V0M.pdb and 3G61.pdb, respectively). In each case, the structure contains the enzyme bound to a known substrate or inhibitor; α-naphthoflavone for CYP1A2, ketoconazole for CYP3A4 and the ligand QZ59 for P-gp. These molecules are used to define a binding site by creating a sphere around each ligand with a radius of 10 Å for the CYP450 enzymes and 20 Å for P-gp. After defining the binding site, the ligands are removed along with all water molecules.

Ligand-enzyme docking was completed using a simulated annealing protocol consisting of 2000 heating steps with a target temperature of 700 K and 5000 cooling steps with a target temperature of 300 K to generate the 10 most favourable docked ligand poses (CDOCKER algorithm). These poses were ranked using the CDOCKER energy and CDOCKER interaction energy parameters (both in kcal/mol). The lowest energy ligand-enzyme complex for each compound was further evaluated by investigating key polar and nonpolar interactions including hydrogen bonding,

electrostatic interactions and van der Waals interactions. This protocol was validated by investigating the binding mode of the known CYP1A2 inhibitor α-naphthoflavone within the CYP1A2 active site and comparing the results with its known crystal structure.[31] Similar protocols were used to investigate the binding interactions of tacrine derivatives with CYP3A4 and P-gp.

3.3 Recombinant CYP450 Assays

The human CYP450 assay kits were obtained from Life Technologies, Burlington, Canada (catalogue numbers P2863 and P2857 for CYP1A2 and CYP3A4, respectively). The assay principle is based on the conversion of a lactone-based substrate into highly fluorescent chromophores by human CYP450 enzyme, which is measured as relative fluorescence units (RFUs). This metabolism converts the substrate from its non-fluorescent blocked form to an extremely fluorescent free form (Figure 9). The reaction was initiated by the conversion of $NADP^+$ to NADPH, which is a necessary co-factor of the fluorescence-generating reaction. Test compounds are evaluated based on their ability to inhibit this fluorescent signal.

Stock solutions of test compounds were prepared in organic solvent dimethyl sulfoxide (DMSO) for CYP1A2 and methanol (MeOH) for CYP3A4, then diluted with phosphate buffer (pH 8.0) to obtain desired concentrations (final test compound concentrations: 0.01, 0.1, 1, 10 and 20 μM; maximum DMSO/MeOH concentration used was 4% v/v). This assay utilizes a solution of microsomes prepared from insect cells that express a single P450 isozyme, CYP1A2 or CYP3A4, and human CYP450 reductase in 100mM potassium phosphate buffer (pH 8.0). Additionally, a regeneration system

consisting of glucose-6-phosphate and glucose-6-phosphate dehydrogenase is required for the conversion of $NADP^+$ to NADPH to initiate the reaction.

Readings were obtained in a black, clear-bottom 96-well plate using a Molecular Devices SpectraMax M5 plate reader in fluorescence mode. For CYP1A2, the excitation and emission wavelengths were 415 nm and 460 nm, respectively; for CYP3A4, the excitation and emission wavelengths were 490 nm and 520 nm, respectively. Each well contains 40 μL of test compound (concentration range used: 0.01-20 μM) and 50 μL of a Master Pre-Mix containing the recombinant enzyme and regeneration system described above. During incubation, a solution of $NADP^+$ and the Vivid® EOMCC (CYP1A2) or DBOMF (CYP3A4) substrate was prepared in supplied reaction buffer. The reaction was initiated by adding 10 μL of the $NADP^+$/substrate mixture to each well and the fluorescence was measured every minute for 15 minutes (Figure 9). A final reading is taken five minutes after the addition of 50 μL of stop reagent (0.5 M tris(hydroxymethyl)aminomethane (tris) base). The assay protocol was validated by preparing a standard curve using a supplied fluorescent standard at various concentrations (0, 7.8, 15.6, 31.2, 62.5, 125, 250, 500 nM; $R^2 = 0.9997$)

Each 96-well plate contains reference agents and controls. For both assays, tacrine was included for comparison. For the CYP1A2 assay, the strong inhibitor α-naphthoflavone was included as a positive control; cimetidine, a weak inhibitor of CYP1A2, was also included as a negative control to compare and validate the results obtained. In the case of CYP3A4, ketoconazole (a strong inhibitor of CYP3A4) served as positive control. Negative controls containing no inhibitor were also included to record 100% CYP450 activity. The degree of inhibition for each compound was calculated as a

half maximal inhibitory concentration (IC_{50}). The experiments were run in triplicate (n = 3) and were reported as the average IC_{50} ± SD of two independent experiments.

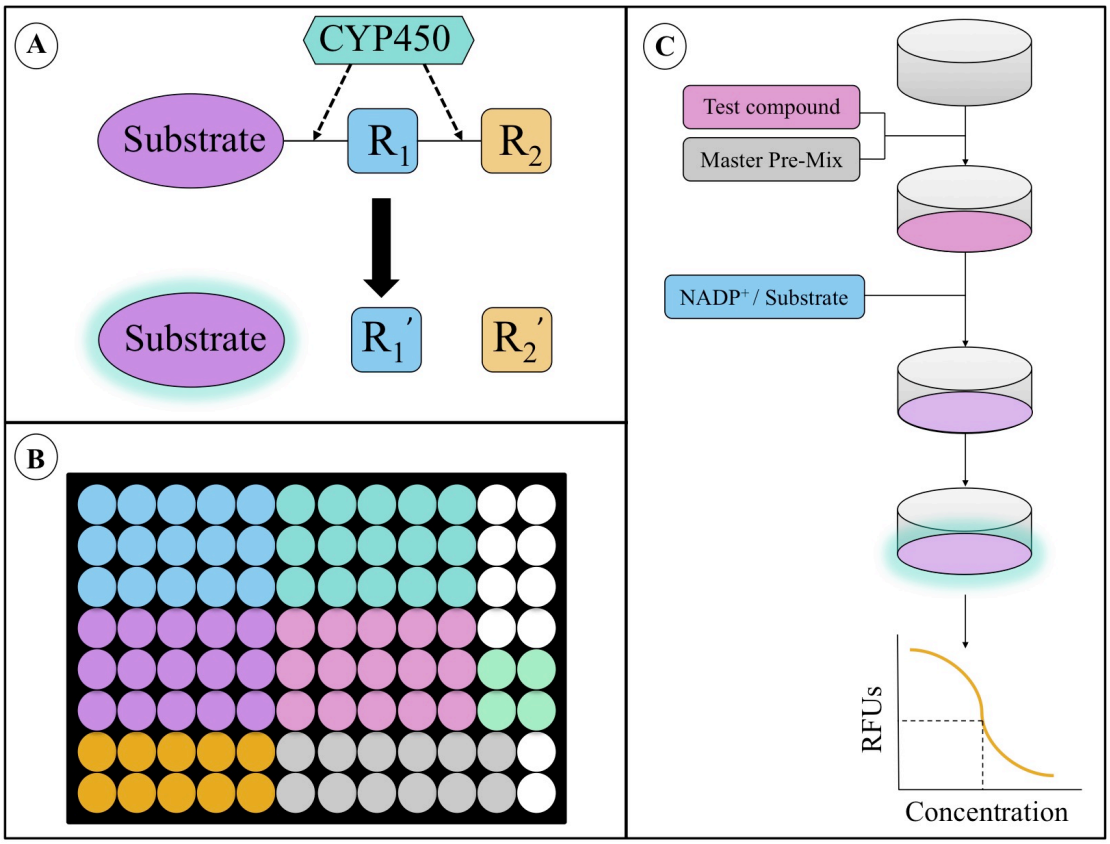

Figure 9. (A) Substrate cleavage by CYP450 produces the highly fluorescent form of the compound, which is detected. (B) A typical 96-well plate for CYP450 assay. The blue, teal, purple and pink wells represent four test compounds at five different concentrations in triplicate, one of which is a control (e.g. α-naphthoflavone). The orange wells represent the negative controls, which contain no test compound. The grey wells contain the highest test compound concentration used in the assay, to confirm there is no interference from the compounds. Similarly, the green wells verify that solvent does not interfere with the fluorescent signal. (C) Addition sequence for CYP450 assay.

3.4 P-glycoprotein Assay

The P-gp (MDR1 or ABCB1) activity was evaluated by detecting the effect of tacrine and its derivatives on recombinant human P-gp in a cell membrane fraction using Pgp-Glo™ assay kit (Promega Corporation, Madison, USA, catalogue number V3601). The assay principle is based on the Pgp/ATPase reaction in the presence of substrate adenosine triphosphate (ATP) and varying concentrations of test compounds. Unmetabolized ATP is detected as a luciferase-generated luminescent signal and measured as relative luminescence units (RLUs) as shown in Figure 10. The stock solutions of tacrine and derivatives were prepared in methanol and diluted with assay buffer to desired concentrations. Each well contains 20 µL of test compound (final concentration range 0.01–100 µM per well), sodium vanadate (positive control), ketoconazole (P-gp inhibitor), verapamil (P-gp stimulant) or phosphate buffer. After adding 20 µL of Pgp membranes, the plates were incubated at 37°C for 5 min. The Pgp/ATPase reaction was initiated by adding 10 µL of substrate Mg-ATP. After 40 minutes of incubation at 37°C, 50 µL of ATP detection reagent was added. The luminescent signals were read every two min. for 40 min. in a clear 96-well plate, using a BioTek Synergy H1 microplate reader. A standard curve was obtained using various concentrations for MgATP (0.37–3.0 mM). The degree of inhibition for each compound was expressed as half maximal effective concentrations (EC_{50} values). The experiments were run in triplicates (n = 3) and were reported as average EC_{50} ± SD of two independent experiments.

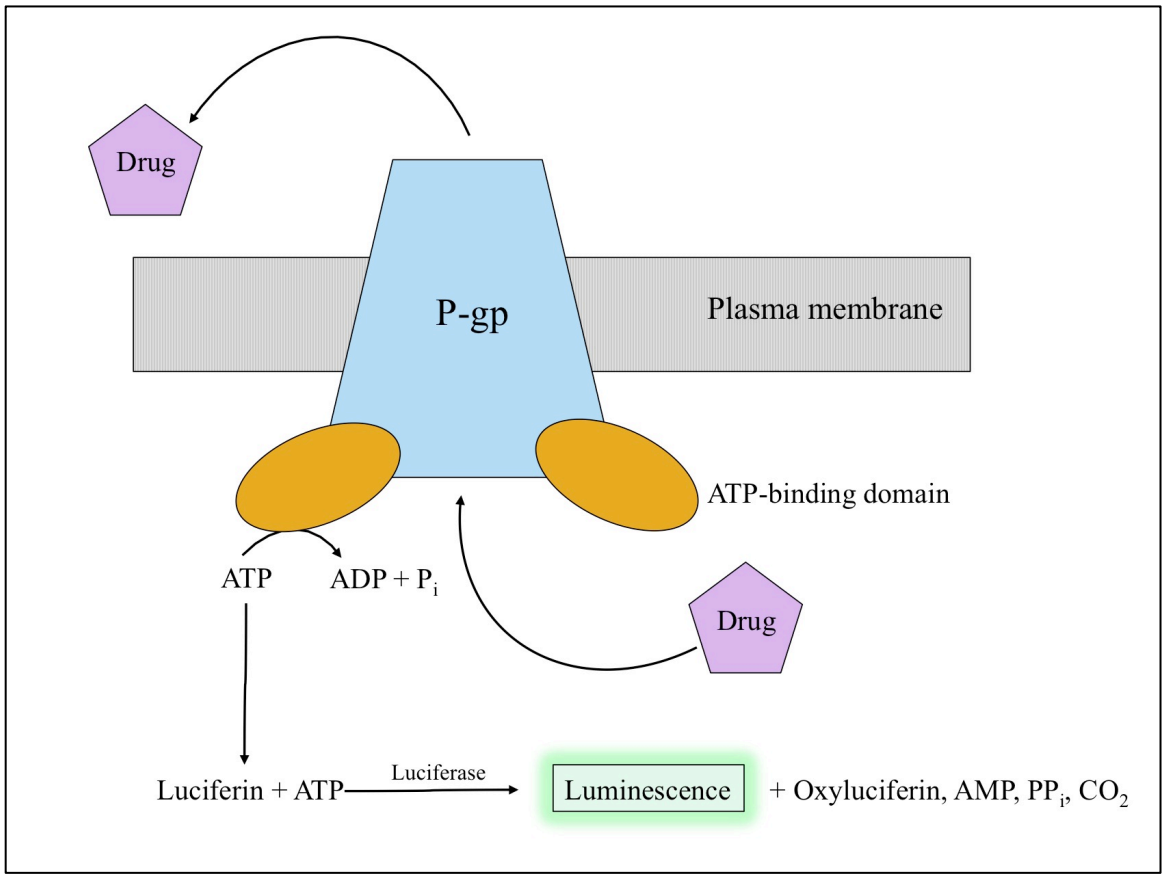

Figure 10. Illustration of ATP-dependent drug transport by P-gp and the subsequent reaction of remaining ATP with luciferin to produce luminescence.

It should be noted that there are several *in vitro* assays that have been used in the classification of P-glycoprotein substrates, including monolayer, calcein-AM and the ATPase assay described above. The monolayer efflux assay measures bidirectional (apical-to-basolateral and basolateral-to-apical) transport across a cell layer. The ratio of these two rates of transport is called the efflux ratio, where a value close to 1 indicates an absence of transport processes. Although this assay provides the most direct manner of measuring efflux, it is also labour-intensive.[68] The calcein-AM[69] and ATPase[70] assays

have similar strengths and weaknesses; they are less tedious, but use an indirect method to measure P-gp transport. Polli and colleagues[71] investigated the concordance between these assays and found that all three methods gave the same result for over half of the compounds tested. By comparing the compounds' apparent permeabilities to their results for the three assays, they were able to determine regions of poor response for each method. For the ATPase assay, this was determined to be compounds with very low permeability (<20 nm per second). Since the compounds we are investigating are small and lipophilic, it is unlikely that we will be in this region and the ATPase assay will correctly identify these compounds are substrates or non-substrates.

3.5 Preparation of Hepatic Microsomes

Rat liver samples were collected from three male Sprague-Dawley rats by Dr. Binbing Ling (University of Guelph). The rats were anesthetised by inhalation of isoflurane. Upon removal, the livers were thoroughly perfused with a buffer containing 1.15% (w/v) potassium chloride (KCl) and 1 mM ethylene diamine tetraacetic acid (EDTA, pH 7.4) until the fluid leaving the tissue was free of blood. This procedure serves to enhance the purity of the microsomal preparations. Following perfusion, the livers were snap-frozen in liquid nitrogen and stored at -80°C until further processing.

The protocol for the preparation of microsomes was adapted from that of Fowler and coworkers (Figure 11).[72] After thawing on ice, the liver samples were weighed and finely minced. Approximately 1 g of liver was transferred to a 7 mL Dounce tissue homogenizer (Bellco Glass, Vineland NJ), to which a homogenization buffer (0.05 M Tris, 150 mM KCl, 0.1 mM Cleland's reagent, 1 mM EDTA and 0.25 mM sucrose) was

added to obtain a 1:4 w/v tissue/buffer ratio. Also, 100 μL of 50 mM phenylmethylsulfonyl fluoride (PMSF) was added. PMSF is a serine protease inhibitor and reduces proteolysis of the desired microsomal protein during preparation. The PMSF solution was prepared fresh daily as its inhibitory behaviour towards proteases quickly decreases if no protease is present (half-life at 25°C, pH 7.0: 110 minutes[73]). Homogenization was achieved through several thrusts with both the large and small clearance pestles. The homogenate was transferred to ultracentrifuge tubes and was centrifuged at 10,400 rpm (10,000 *g*) for 20 minutes at 4°C in a Beckman Coulter 70.1 Ti fixed angle rotor. The supernatants from these preparations were collected and transferred to new ultracentrifuge tubes and centrifuged at 34,000 rpm (100,000 *g*) for 60 minutes at 4°C in the same Beckman Coulter rotor as previously. When the run was complete, the supernatants were discarded and the pellet was washed in 0.1 M phosphate buffer and centrifuged again at 34,000 rpm for 60 minutes at 4°C. After this final spin, the supernatants were again discarded and the remaining pellet was reconstituted in a storage buffer containing 0.05 M tris and 1 mM EDTA in 20% glycerol such that 1 mL of the suspension contained material from 0.5 g of liver. These samples were separated into 1.5 mL aliquots and were stored in Eppendorf tubes at -80°C until further use.

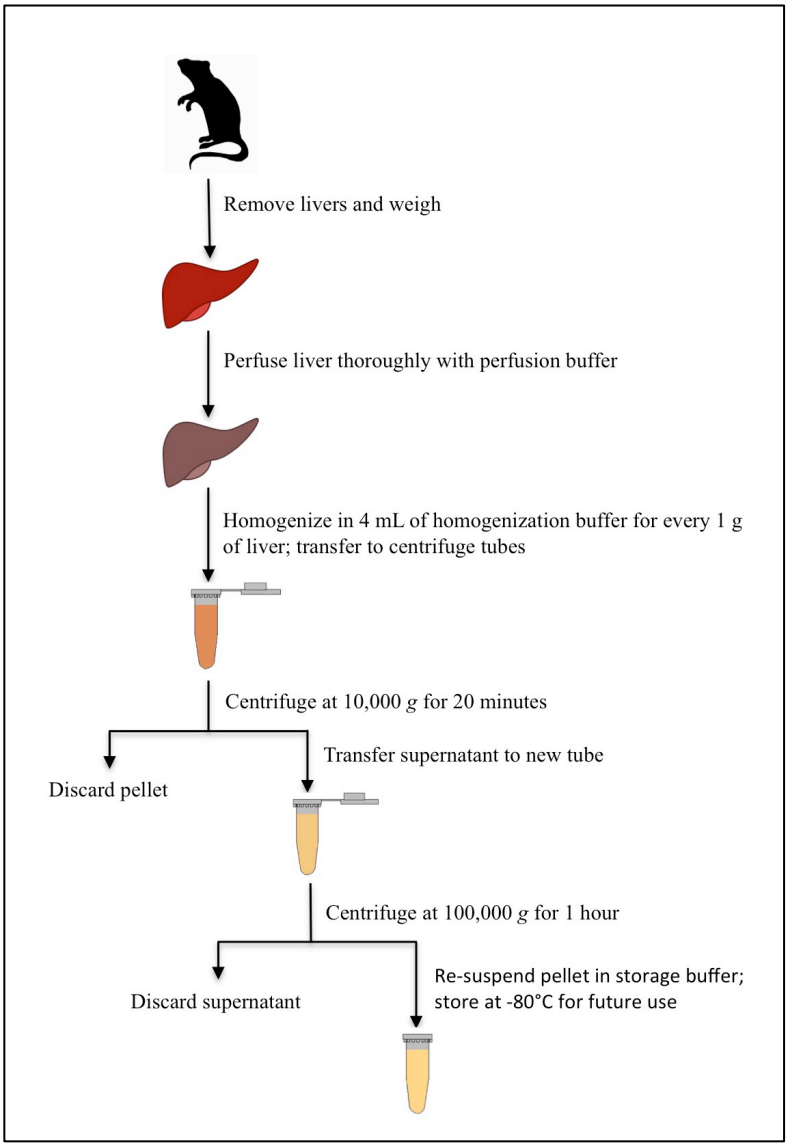

Figure 11. Experimental flow chart summarizing the isolation of hepatic microsomes

3.5.1 Protein Quantification

The method used to quantify the protein present in the microsomal samples was first described by Bradford in 1976.[74] This assay employs the Coomassie Brilliant Blue G-250 dye, which exists in cationic, neutral and anionic forms (Figure 12). These species

display maximum absorbance at 470 nm (red), 650 nm (green), and 595 nm (blue), respectively. In the acidic environment of the Coomassie dye, the anionic species is not present in its free form; as a result, the solution – a mixture of the red cationic and green neutral forms – appears brown. However, it is the anionic form that binds to protein; this species undergoes significant electrostatic interactions with the positively charged amino acid residues arginine, lysine and histidine, as well as van der Waals interactions with aromatic residues.[75] As the anionic form binds to protein, its free concentration decreases and the equilibrium favours further production of the anionic species. As a result, protein binding causes an increase in absorption at 595 nm and it is this absorbance that is measured to quantify the protein content of a sample.

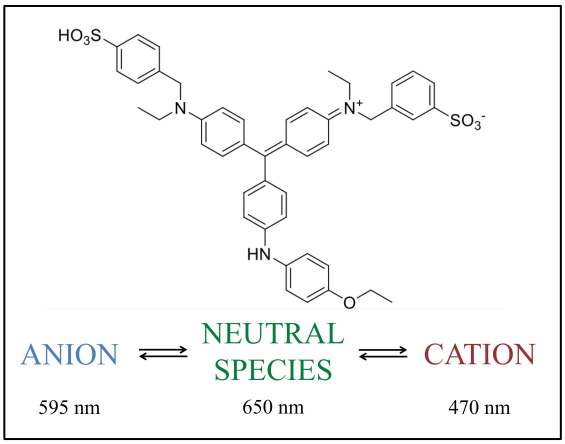

Figure 12. Chemical structure of the Coomassie dye and the wavelength of maximum absorbance for its various species.

The Coomassie Protein Assay Kit was obtained from Thermo Scientific and included 2 mg/mL bovine serum albumin, which was used to prepare a calibration curve from 0.1 mg/mL to 1.5 mg/mL. A sample from each rat was serially diluted up to a 160x

dilution to ensure overlap with the linear range of the standard. Readings were obtained in a clear 96-well plate using a BioTek Synergy H1 microplate reader in absorbance mode. Each well contained 5 μL of either albumin standard or microsomes and 250 μL of the Coomassie reagent. All samples were present in triplicate, and were allowed to incubate for 15 minutes before absorbance at 595 nm was recorded using a Biotek Synergy Neo Multi-Mode Reader. A linear least squares fit was used to produce the equation for the calibration curve (R^2 = 0.9857). Measurements for the microsomal samples were compared to the calibration curve and averaged to determine the protein content for each rat.

3.5.2 Cytochrome P450 Reductase Activity

Cytochrome P450 reductase is a membrane-bound protein found in the endoplasmic reticulum and is essential to the metabolic processes catalyzed by the cytochrome P450 enzymes. Cytochrome P450 reductase supplies the cytochrome P450s with the electrons needed for this catalytic activity, with NADPH serving as the source of electrons. A typical P450 reaction can be written as follows:

$$RH + O_2 + NADPH + H^+ \rightarrow ROH + H_2O + NADP^+$$

where RH is the substrate that is oxidized by the P450, making it more hydrophilic and therefore more easily eliminated by the kidneys.[76]

Prior to conducting metabolism studies, it is essential to verify that this electron transfer is taking place. To do so, a spectrophotometric titration is performed using a surrogate electron acceptor; in this study, potassium ferricyanide is employed, but 1,1-diphenyl-2-picrylhydrazyl and cytochrome *c* can also be used for this purpose.[77] A

Master Mix containing 0.625 mM potassium ferricyanide and a 1 mM stock solution of NADPH (final concentrations 0.5 mM and 0.1 mM, respectively) were prepared in 0.3 M phosphate buffer (pH 7.4). Protein samples from each rat were standardized to 4 mg/mL, then serially diluted in phosphate buffer to produce 2x, 4x, 8x, 16x and 32x dilutions. This assay was performed in a clear 96-well plate, with each well containing 10 µL of microsomes and 80 µL of the Master Mix. After recording baseline absorbance at 420 nm for 3 minutes, 10 µL of the NADPH solution was added to each well to initiate the reaction. Absorbance at 420 nm was recorded for another 3 minutes. Each diluted sample was present in triplicate, and blanks containing no microsomes and no NADPH were also included. The rate of ferricyanide reduction (r, in mM min^{-1}) was calculated using the following equation, a rearrangement of the Beer-Lambert Law:

$$r = \frac{\Delta A_{420}\, min^{-1}}{\varepsilon \cdot \ell}$$

where ΔA_{420} is the change in absorbance at 420 nm per minute, ε is the extinction coefficient for potassium ferricyanide (1.02 mM^{-1} cm^{-1}) and ℓ is the path length (i.e. the depth of the reaction mixture within the well, or 0.296 cm).

3.6 Measurement of *In Vitro* Intrinsic Clearance

3.6.1 Substrate Depletion Studies

Before completing the substrate depletion experiments, incubations at a single concentration were conducted to identify metabolites and ensure appropriate reaction conditions. In an Eppendorf tube, 500 µM test compound was combined with 2 mg/mL microsomal protein and heated to 37°C. To initiate the reaction, NADPH was added to

the reaction mixture for a final concentration of 1 mM. After 24 hours, the reaction was terminated by addition of 250 µL of ice-cold acetonitrile. After 20 minutes of centrifugation at 13,000 *g*, the supernatant was passed through a 0.45 µm filter and the mass of metabolite(s) was determined using an Agilent 1260 infinity series LC-MS (see Table 1).

Table 1. LC-MS conditions for analysis of tacrine and derivatives.

Column	Agilent Poroshell 120 EC-C18 (4.6 x 50 mm, 2.7 µm)
Mobile Phase	70% water / 30% acetonitrile with 0.1% TFA
Injection Volume	10 µL
Flow rate	0.5 mL/min
Detector Wavelength	254 nm

Substrate depletion studies were carried out in 96-well plates, with one row designated for one of five concentrations (range: 1-500 µM, Figure 13). Each well contained 40 µL of test compound, 50 µL of microsomes from Rat #2 and 90 µL of 0.3 M phosphate buffer. The plate was incubated at 37°C with shaking, and the reaction was initiated by addition of 20 µL of NADPH, bringing the total reaction volume to 200 µL. Reactions were terminated at specified times (0, 2, 5, 10, 15, 30, 60, 90, 120, 180, 210 and 240 minutes) by addition of 100 µL of ice-cold acetonitrile. Samples were processed as outlined above. The concentration measured by LC-MS for the t = 0 samples is considered to be 100% substrate and measurements at later time points are recorded as a percentage of this value.

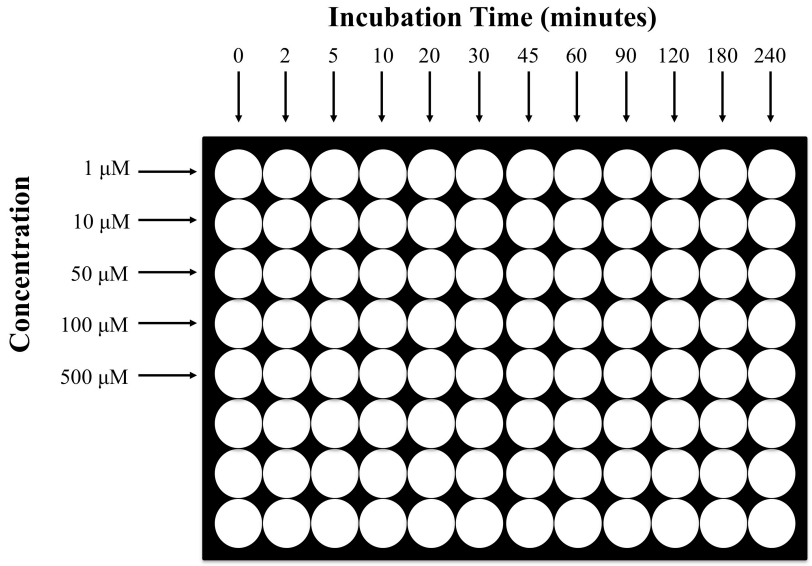

Figure 13. Sample 96-well plate setup for substrate depletion studies.

The data for each concentration was fit to the following equation:

$$\%S_t = e^{-k_{dep} \times t}$$

where $\%S_t$ is the percentage of substrate remaining at time *t* and k_{dep} is the depletion rate constant. After fitting this equation to each substrate concentration, the data was fit to the following equation:

$$k_{dep} = k_{dep([S]\rightarrow 0)}\left(1 - \frac{[S]}{[S] + K_m}\right)$$

where $k_{dep([S]\rightarrow 0)}$ is the theoretical rate constant for an imperceptibly low concentration of substrate and K_M is the Michaelis-Menten constant, which describes the likelihood that a compound will saturate a particular metabolic pathway. Finally, $k_{dep([S]\rightarrow 0)}$ was scaled to intrinsic clearance using a physiologically based scaling factor.

3.6.2 Microsomal Binding Assays

Microdialysis experiments were conducted to determine the extent of binding to microsomal protein in the substrate depletion studies. Before performing microdialysis, a calibration curve was prepared for each compound in phosphate buffer (pH 7.4). The wavelength of maximum absorbance for each compound was determined by conducting a sweep of the UV-visible spectrum and any interference from 100 μM ketoconazole at these wavelengths was noted. Protein binding experiments were carried out using the QuixSep™ Micro Dialyzer system with a regenerated cellulose membrane (nominal molecular weight cut-off: 12,000-14,000 Da; Membrane Filtration Products Inc., Seguin, Texas, USA). The protein and test compound are contained in the chamber (total volume: 500 μL; test compound concentration: 4000 μM; protein concentration: 2 mg/mL), which is then placed in a beaker containing phosphate buffer with 0.9% NaCl (w/v%). Ketoconazole (100 μM) was also included in these assays to rule out any CYP3A4 binding. The inhibitor was added before the test compound and was allowed to incubate with the protein for 15 minutes. After seven hours of dialysis, the sample was aspirated from the chamber. The UV absorbance was recorded for both sides of the membrane, and the extent of protein binding was calculated as follows:

$$\%\ Protein\ Binding = 100 \times \frac{C_{protein} - C_{buffer}}{C_{protein}}$$

3.7 Development of Rat PBPK Models for Tacrine and Derivatives

3.7.1 Software Used

All PBPK models were created using the software PK-Sim® (version 5.5; Bayer Technology Services GmbH, Leverkusen Germany). This software generates models with a total 17 compartments representing organs and tissues, which are further divided into sub-compartments of red blood cells, plasma, interstitial space and cellular space. The compartments are connected via blood flows, with the system being closed via the lung (Figure 14). These models incorporate anatomical and physiological parameters for humans and several commonly used preclinical animals. For each organism, the software includes databases to describe how these parameters depend on the weight and/or height of the organism. Using compound-specific physicochemical properties such as lipophilicity, plasma protein binding and molecular weight, PK-Sim® uses referenced and proprietary algorithms to provide estimates of absorption and distribution parameters such as organ-plasma partition coefficients and intestinal and cellular permeability.

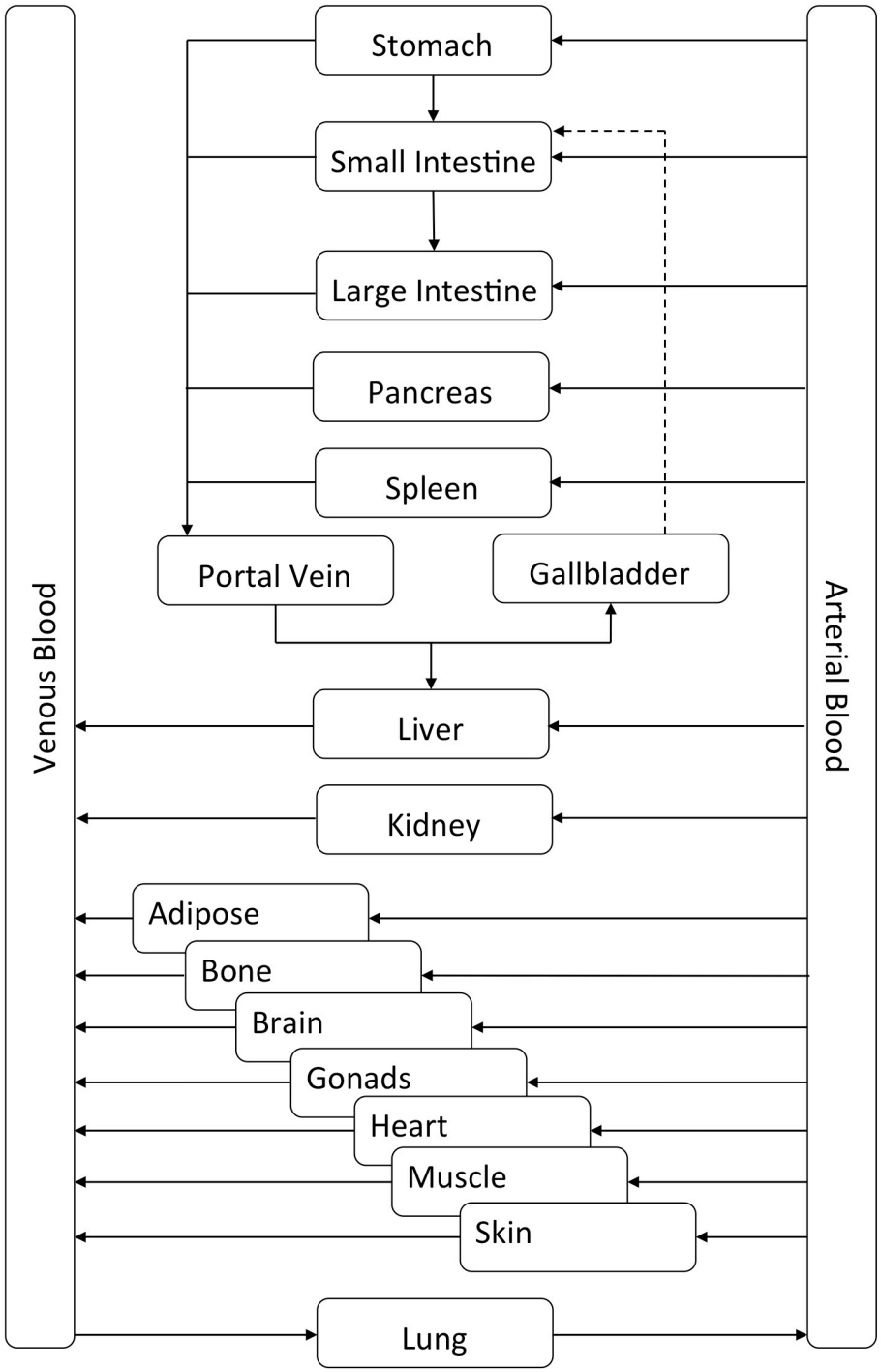

Figure 14. Whole body PBPK model structure illustrating the 17 organ compartments and the venous and arterial blood flows that connect them.

3.7.2 Workflow for PBPK Model Development

Before developing models for the novel tacrine derivatives, a PBPK model for tacrine was first created (Figure 15). Several *in vivo* studies have been conducted with tacrine in rats, and the ability to compare simulated and observed concentration-time profiles offers the opportunity to optimize parameters and gain a more complete understanding of all processes influencing the absorption, distribution and elimination of tacrine. This type of comparison is not possible with the other compounds explored in this project as no *in vivo* studies have been conducted.

The initial tacrine model combines the rat-specific anatomy and physiology included in PK-Sim® with physicochemical and ADME data found in the literature. Concentration-time profiles were generated and compared to the *in vivo* rat data. In the case of considerable discrepancy between the simulated and observed data, uncertain model parameters such as permeability, clearance and transport activity were optimized until an acceptable goodness-of-fit was achieved. Particular emphasis was placed on achieving good fit for the curve representing unbound concentration in the brain interstitial space, as brain intracellular concentrations (where acetylcholinesterase is located) are used to determine dose.

Once the tacrine model was been optimized, the models for its derivatives could be developed. These models incorporated the same rat-specific parameters as the previous model, but used the data gathered from *in silico* and *in vitro* experiments for the compound-specific inputs such as lipophilicity, pK_a, molecular weight, and intrinsic clearance. Although it was not possible to optimize derivative parameters by comparing to observed data, any optimized parameter from the tacrine model was similarly modified

from PK-Sim-estimated for the derivatives parameters. For example, PK-Sim® provides estimates of cellular and endothelial (in the case of the BBB) permeability based on the compound's lipophilicity and effective molecular weight but the optimal value for permeability may differ from this estimate. When this situation arose, the ratio of the optimal to the estimated value for tacrine was used to scale the estimated values for the derivatives. When the models for the derivatives were fully parameterized, the dose was adjusted such that the desired brain concentrations were achieved. Target concentrations were defined as the concentration that inhibited 90% of AChE activity *in vitro* (AChE IC_{90}).

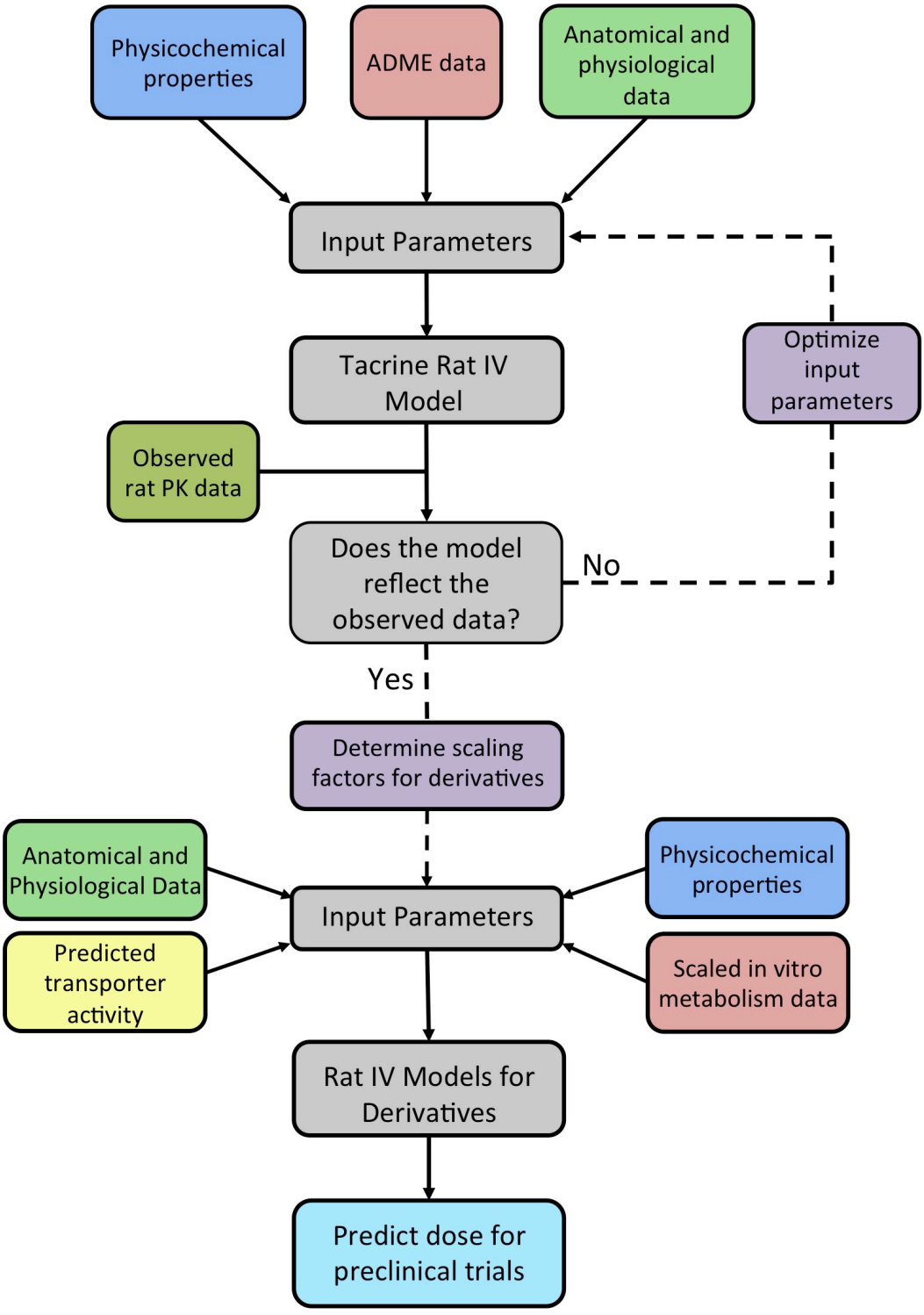

Figure 15. Workflow for development of PBPK models for tacrine and derivatives.

3.7.3 Development of Rat PBPK Model for Tacrine

A rat PBPK model was created for tacrine based on a study conducted by Telting-Diaz and Lunte,[78] in which Sprague-Dawley rats were dosed with 1 mg/kg of tacrine intravenously and tacrine concentrations were measured both in blood and in brain interstitial space by microdialysis. The generic individual rat in PK-Sim has a body weight of 227.8 g, which was not representative of those used in the study (weight range 350-450 g). The body weight was manually adjusted and all organism specific anatomy and physiology, such as organ volumes, blood flow rates were scaled accordingly by PK-Sim. Physicochemical properties were obtained from the literature, including the blood-to-plasma ratio (B:P), which was calculated using protein binding data from Telting-Diaz and Lunte, and the equation below:[79]

$$f_{u,p} \times C_p = f_{u,b} \times C_b$$

$$B{:}P = \frac{C_b}{C_p} = \frac{f_{u,p}}{f_{u,b}} = \frac{1 - 0.562}{1 - 0.733} = 1.64$$

CYP1A2 is the only major enzyme in tacrine metabolism, accounting for 90% of tacrine clearance.[28] In the preliminary model, clearance was attributed entirely to CYP1A2, with an arbitrary initial input of CL_{int} = 1 L/min. Following simulation, the experimentally derived data for both blood and brain (interstitial unbound brain concentration) were superimposed onto the simulated concentration-time profiles. Because this model did not adequately reflect the observed data, parameters of clearance and distribution were optimized. The total blood clearance was slightly underestimated in the initial model, hepatic clearance via CYP1A2 being blood flow limited at 1 L/min.

Because CL_{int} is not identifiable in a blood flow limited situation using optimization, hepatic CL_{int} was reduced to the lowest value that did not result in a perceptible change in curve shape (0.7 L/min). Since clearance was underestimated, other clearance pathways were investigated. Evidence from the literature suggests that only a very small fraction of the tacrine dose is removed by urinary excretion in humans (0.5% of dose[80]). A similar estimate is not available for rats; as a result, glomerular filtration was the only renal clearance process incorporated into the model where renal clearance due to glomerular filtration was the fraction unbound in plasma multiplied by the glomerular filtration rate (fraction excreted unchanged in urine = 0.03). Once blood clearance was reasonable, brain concentrations were assessed for predictive accuracy with observed data. The simulation underestimated the extent of tacrine distribution into the brain (simulated C_{max}: 0.115 μM; observed C_{max}: 0.20 μM) and so an influx transporter representing organic cation transporter 2 (OCT2), a known tacrine transporter,[81] was incorporated into the blood-brain barrier to facilitate brain uptake. While the K_m of the transporter is unknown, it is in the range of 0.02-4.3 μM, since researchers determined that this was the range of tacrine blood concentrations where brain uptake was saturable.[81] For the purposes of modelling, a mid-range value of 1 μM was selected as the K_m. Transport was parameterized with Michaelis-Menten type kinetics and V_{max} was manually optimized using the observed brain data to 1.0 μmol/mL/min. Another discrepancy between the simulated and observed data was the rate of distribution into the brain, which was highly overestimated by the model; brain concentrations were predicted to be proportional to blood concentrations almost immediately whereas observed data showed that brain concentration did not come into equilibrium with blood until 0.6 h

post-administration. To improve curve shape at early time points, the permeability between plasma and brain interstitial space was decreased from 0.44 cm/s to 0.003 cm/s. Adjustment of these two parameters produced a brain concentration-time profile that reflected the experimental data reasonably.

3.7.4 Development of Rat PBPK Models for Tacrine Derivatives

Upon fully parameterizing the tacrine model, analogous models were created for the tacrine derivatives using the same rat-specific anatomical and physiological parameters combined with predicted physicochemical and ADME data from *in silico* and *in vitro* experiments. ClogP was estimated using the ChemDraw Ultra software (version 11.0, Cambridge Software Company) and pKa was determined in the *Calculate Molecular Properties* module of Discovery Studio. Fraction unbound was maintained at the same value as tacrine for all derivatives and $CL_{int,s}$ were determined through *in vitro* experimentation.

As mentioned previously, tacrine is known to be a substrate for the transporter OCT2 and the inclusion of this transport process was needed to achieve the observed concentrations in brain. The crystal structure of OCT2 has not yet been solved, and as a result, molecular docking studies similar to those conducted for P-gp were not possible. However, a number of studies using pharmacophore modelling have been conducted for OCT2 and a number of physicochemical properties influencing OCT2 substrate behaviour have been identified. By comparing the derivatives with tacrine for each of these properties, the likelihood that these compounds would also be OCT2 substrates was assessed.

Chapter 4.0 Results and Discussion

4.1 Initial Compound Selection

Before beginning the *in vitro* experiments, 25 compounds were screened using existing target affinity data and calculated lipophilicity. Although several of the compounds displayed dual cholinesterase inhibition, an emphasis was placed on potency towards AChE. Under normal physiological conditions and in early stages of AD, AChE takes on the primary role in ACh hydrolysis and is present at a concentration four times greater than that of BuChE; it is not until late stages of AD the BuChE becomes the prominent catalyst for ACh degradation.[82] The majority of compounds eliminated during this step (n = 7) belonged to Class A (containing no halogen on the tetrahydroacridine ring); in fact, all of the compounds from Class B (compounds chlorinated at the C-6 position) were considered for further investigation. This suggests that the inclusion of a chloro group on the tetrahydroacridine ring at the C-6 and C-7 positions enhances affinity for AChE. However, the addition of a chloro group also increases a compound's lipophilicity by 0.81 units, bringing many of the Class B and C compounds into an undesirable range of lipophilicity (Table 2) and potentially increasing the risk of toxicity. High lipophilicity resulted in the elimination of 9 compounds, leaving 9 compounds for further investigation. The majority of these compounds contain either a 3,4-dimethoxybenzyl or a picolyl moiety at the C-9 position, suggesting that these groups not only convey target affinity, but are also hydrophilic enough to balance the effects of the chloro group on overall lipophilicity.

Table 2. Existing data used to select compounds for further investigation.

	Physicochemistry			Cholinesterase Inhibition (μM)[a]		Aggregation Inhibition[b]	
Compound	MW	ClogP[c]	N + O[d]	AChE	BuChE	$A\beta_{1-40}$	$A\beta_{1-42}$
A1	288.39	5.52	2	6.96	0.41		
A2	318.42	5.44	3	5.81	0.09		
A3	318.42	5.44	3	3.34	0.08		
A5	348.42	5.18	4	2.23	0.02	59.8%	24.8%
A6	362.42	5.83	4	4.57	0.08	41.1%	21.0%
A7	289.38	4.02	3	6.65	0.07		
A8	289.38	4.02	3	3.99	0.22		
B1	323.85	6.33	2	1.67	3.99		
B2	353.87	6.25	3	2.98	2.38		
B3	353.87	6.25	3	0.61	5.22		
B4	353.87	6.25	3	0.72	9.10		
B5	383.89	5.99	4	0.85	1.40	64.8%	41.6%
B6	397.87	6.64	4	0.63	1.86	65.7%	20.7%
B7	324.38	4.83	3	0.10	1.61		
B8	324.38	4.83	3	0.19	12.73		
B9	324.38	4.83	3	0.03	1.37		
C1	323.85	6.33	2	2.59	12.11		
C2	353.87	6.25	3	5.10	4.25		
C3	353.87	6.25	3	1.89	8.25		
C4	353.87	6.25	3	3.37	11.65		
C5	383.89	5.99	4	1.26	9.27	77.3%	28.3%
C6	397.87	6.64	4	3.17	7.27	35.9%	40.5%
C7	324.83	4.83	3	7.06	6.78		
C8	324.83	4.83	3	7.69	>25		
C9	324.38	4.83	3	3.06	4.69		
Tacrine	198.27	3.27	2	0.215	0.05		

[a]IC_{50} values are the average of two to three separate experiments (n = 3) with mean deviation of less than 10%. [b]Aggregation inhibition is reported as percent inhibition of the peak value (t = 6 hours) by 5 μM test compound and is the average of two separate experiments (n = 3). [c]ClogP was determined using ChemDraw Ultra (version 11.0, Cambridge Software Company). [d]N + O is the number of nitrogen and oxygen atoms and gauges potential for hydrogen bonding.

4.2 Tacrine and its Derivatives as Substrates for CYP1A2

4.2.1 Validation of CYP1A2 CDOCKER Protocol

To validate the docking protocol before its use on the novel derivatives, the co-crystallized ligand (i.e. α-naphthoflavone) was docked into the specified binding sphere. The accuracy of the docking was assessed using the root mean square deviation between the heavy atoms of the co-crystallized ligand and those in the most favourable docked position.

$$root\ mean\ square\ deviation = \sqrt{\frac{1}{N}\sum_{i=1}^{N}\delta_i^2}$$

In the above formula, δ_i is the distance between the ith corresponding heavy atoms and N is the total number of heavy atoms. The distances between corresponding atoms were between 0.225 and 0.455 Å and the root mean square deviation was 0.323 Å, well below the threshold required for docking to be considered successful (1.0-3.0 Å).[83,84]

4.2.2 Evaluating Tacrine and its Derivatives as CYP1A2 Substrates

The most favourable pose for tacrine docked within the CYP1A2 binding site shows a position similar to that of α-naphthoflavone, where the tetrahydroacridine ring system is inserted between the Gly316-Ala317 backbone and the Phe226 residue, allowing several π-π stacking and π-amide stacking interactions to occur (distance < 4 Å). A hydrogen bond forms between a NH_2 hydrogen and the C=O of Asp320 (distance = 2.3 Å), and several van der Waal's interactions were seen with Ala317 and Leu497 (distance < 5 Å). This pose also shows tacrine oriented with the cyclohexene ring

positioned closest to the heme group, which is most amenable to the formation of the major metabolite, 1-hydroxytacrine, as well as the minor products 2- and 4-hydroxytacrine. However, the fifth and sixth most favourable positions show tacrine positioned with the benzyl ring nearest to the heme group, which would allow the formation of the 7-hydroxytacrine metabolite and subsequent production of toxic intermediates.

In addition to the ability to observe a molecule's position within a binding site, the Discovery Studio software also provides numerical scoring functions to quantify the stability of the ligand-enzyme complex and the affinity of the ligand for that enzyme. These parameters are called the CDOCKER energy (CDE) and CDOCKER interaction energy (CDIE), respectively. The CDIE reflects the affinity of a ligand for a protein, while the CDE incorporates both the interaction energy and the internal ligand strain energy to measure the stability of the ligand-protein complex. The most favourable pose for tacrine had CDE = -21.90 kcal/mol and CDIE = -35.16 kcal/mol. Tacrine's affinity for CYP1A2 was also investigated in an *in vitro* setting, using a fluorescence-based recombinant CYP1A2 assay. From these experiments, tacrine was found to have a CYP1A2 IC_{50} of 1.483 ± 0.31 μM. This strong affinity for CYP1A2 correlates well with the energy parameters and the large number of close interactions with residues in the CYP1A2 active site.

In order to gain more insight into which pharmacophores are most desirable for increasing or decreasing CYP1A2 affinity, docking experiments were conducted for the full library of compounds and the following trends were observed. Firstly, the Phe226 and Gly316-Ala317 backbone prove critical in CYP1A2 substrate binding as all

compounds interacted with these residues, regardless of their orientation within the binding site. These interactions consisted of stabilizing π-π stacking, π-amide stacking, and π-alkyl interactions with either the aromatic C-9 substituent or the tetrahydroacridine ring system. Additional π-alkyl interactions with Ala317 and Leu497 are also observed for all compounds, as well as π-π T-shaped interactions with the heme prosthetic ring. In addition to these interactions common to all compounds, each class of compound also undergoes distinctive contacts with surrounding residues. For example, the addition of a chlorine group at C-6 (i.e. Class B compounds) results in close van der Waal's contact with Ser122 while the same substitution at C-7 (i.e. Class C compounds) promotes interaction with the Thr223 and Asp320 residues. Furthermore, there is a distinct trend when comparing the complex stability of corresponding compounds across the three classes (Figure 16). With the exception of the compounds with substituents **5** (3,4-dimethoxybenzyl, Figure 6) and **6** (3,4-dimethoxyphenethyl, Figure 6), the CDE increases moving from Class A to Class C, differing by +9.11 kcal/mol on average. This suggests that the addition of a chlorine atom at the C-7 position has a significant impact on the internal ligand strain energy and results in a reduction in complex stability. A similar effect is observed for the Class B compounds, where the chlorine atom is at the C-6 position, but to a lesser degree (average increase in CDE: +5.09 kcal/mol).

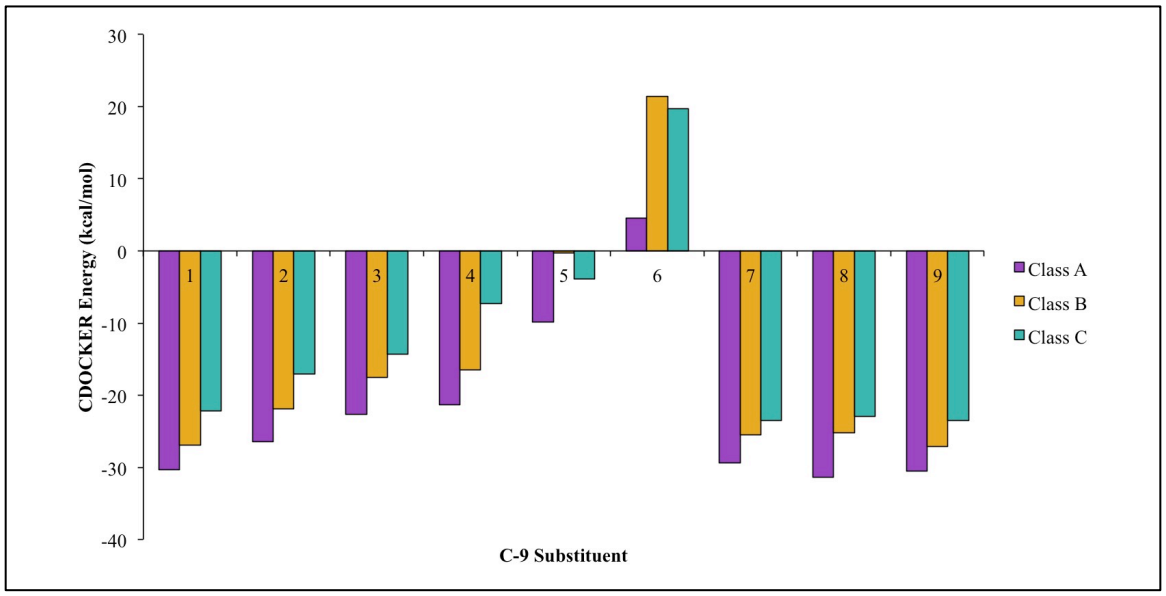

Figure 16. Trends in CDOCKER Energy of CYP1A2 complexes for different C-9 substituents across the three compound classes.

The type of substituent at the C-9 position also impacts the way in which a compound binds to CYP1A2, which can be easily seen by dividing the compounds into two series: (i) substituted benzylamine series (R-groups **1**-**6**) and (ii) picolylamine series (R-groups **7**-**9**). From Figure 17, the addition of a substituted benzylamine group tends to increase CYP1A2 IC_{50}, especially when this group becomes large in size (R-groups **5** and **6**). This effect is likely due to the narrow binding site of CYP1A2. As mentioned, the total active site volume for this enzyme is approximately 375 $Å^3$ and typical CYP1A2 substrates have molecular volumes below 200 $Å^3$. The molecular volumes of the compounds containing a 3,4-dimethoxybenzylamine moiety approach 300 $Å^3$. On the other hand, a picolylamine-substituted compound (which has a molecular volume of less than 215 $Å^3$) shows CYP1A2 affinity equal to or higher than that of tacrine. The high

affinity of these picolylamine-containing compounds can be attributed to coordination between the picolyl nitrogen and the heme iron atoms. This effect is known as type II binding and is known to slow the catalytic action of various CYP450s by preventing the binding of oxygen to the heme, which can greatly enhance a drug's metabolic stability.[85] These interactions have been studied in depth by Jones and coworkers, who investigated a number of groups containing sp^2-hybridized nitrogen atoms and their ability to interact with heme iron using density functional theory calculations to quantify affinity for coordination.[86] This study also corroborated an *in vitro* observation that found replacement of the pyridine nitrogen in nicotine with a carbon atom reduced binding to the bacterial oxygenase CYP101A1 by more than 250-fold.[87]

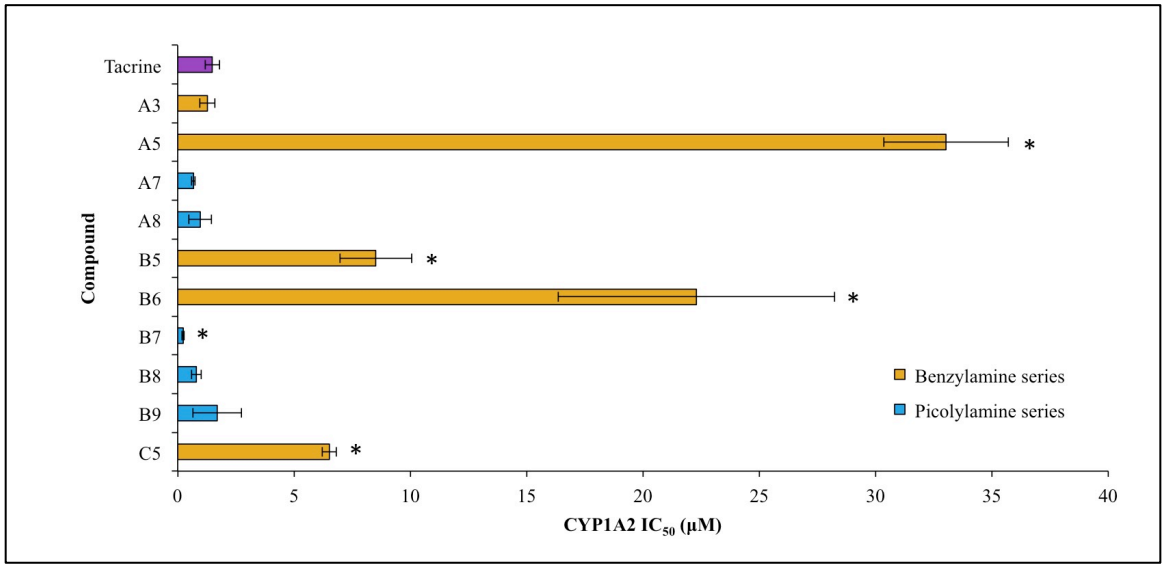

Figure 17. CYP1A2 IC_{50} values for selected compounds. Results are expressed as mean ± SD (n = 3) for two independent experiments. *$p < 0.05$, unpaired Student's *t*-test.

In order to most effectively prevent the formation of toxic species, we sought to eliminate any compounds that were not oriented with the C-9 substituent closest to the heme group for each of the ten most favourable conformations. This strict condition should not only prevent the direct production of the harmful 7-hydroxytacrine species, but also reduce the possibility of the formation and subsequent rearrangement of 1-, 2-, or 4-hydoxytacrine.

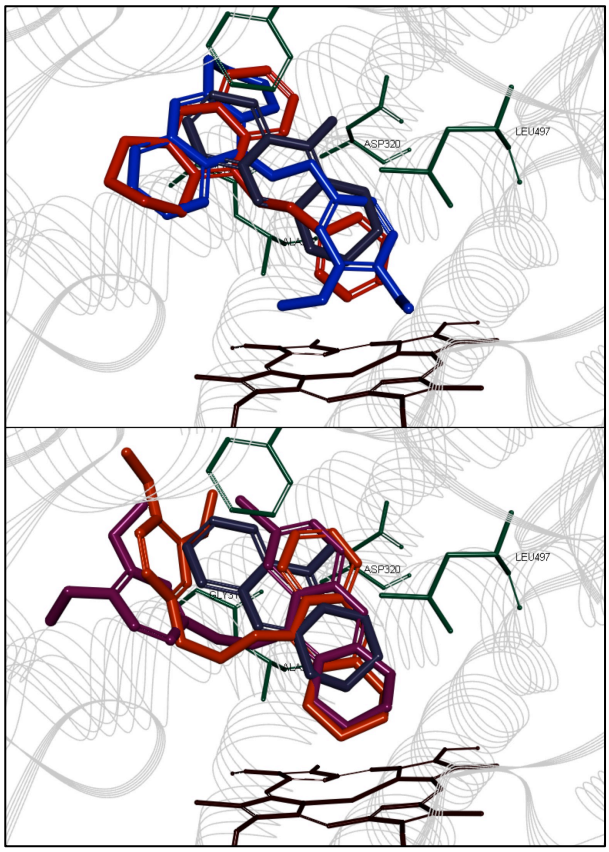

Figure 18. Top: Tacrine derivatives oriented with the C-9 position close to the CYP1A2 heme group. Bottom: Tacrine derivatives docked in an unfavourable orientation. *Grey:* tacrine; *red:* A8; *blue:* A5; *orange:* A6; *maroon:* C5.

Only compounds A3, A5, B5 and A8 were docked in this position consistently. A more detailed inhibition profile for tacrine and these four derivatives is shown in Figure 19.

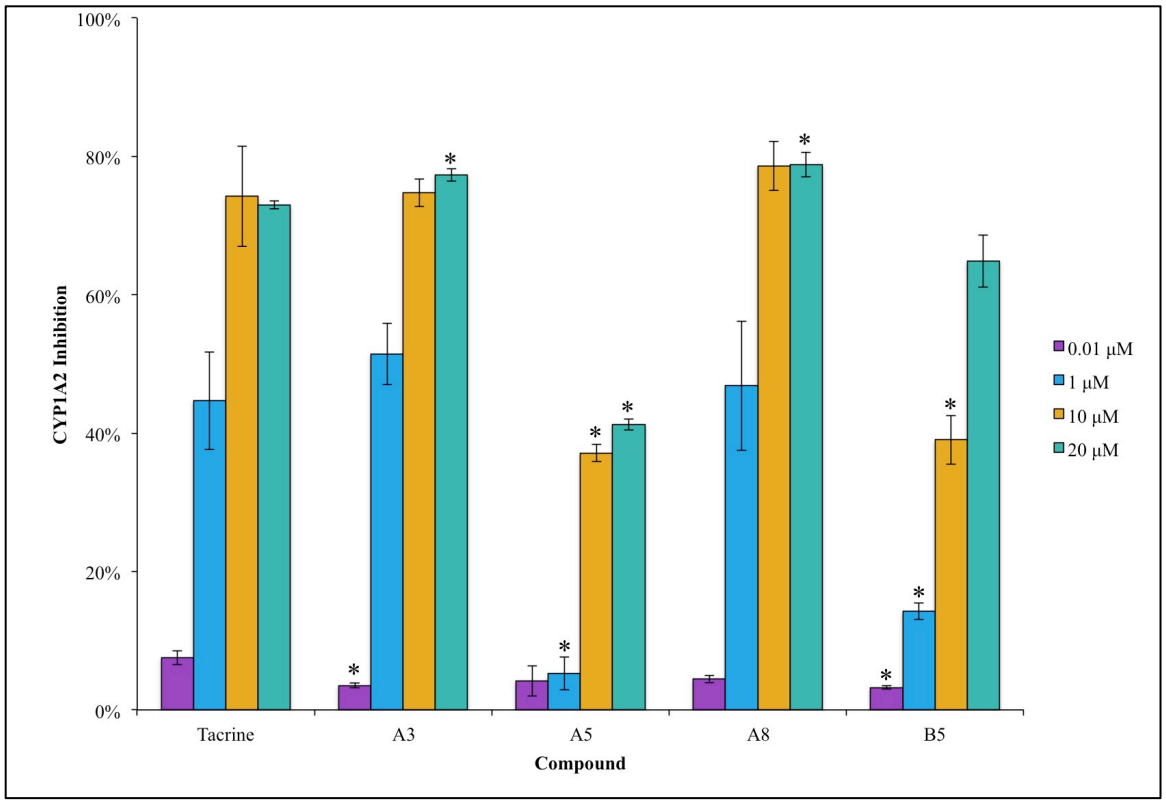

Figure 19. CYP1A2 inhibition profile of tacrine, A3, A5, A8 and B5 at increasing concentrations (0.01 – 20 µM). Results are expressed as % inhibition ± SD (n = 3) for two independent experiments. *$p < 0.05$, unpaired Student's *t*-test.

4.2.3 Correlation of *In Vitro* and *In Silico* CYP1A2 Data

The *in vitro* CYP1A2 assays provide a measure of the affinity of a compound for CYP1A2 by evaluating its ability to inhibit the metabolism of a known CYP1A2 substrate. *In silico* docking experiments also estimate affinity by calculating the stability

of the ligand-enzyme complex. Although *in vitro* data is most commonly extrapolated to predict *in vivo* PK, the use of computational modelling techniques are gaining popularity as a more economic and less labour-intensive option. In light of this trend, the correlation between estimated compound-CYP1A2 complex stability and *in vitro* CYP1A2 IC_{50} was investigated.

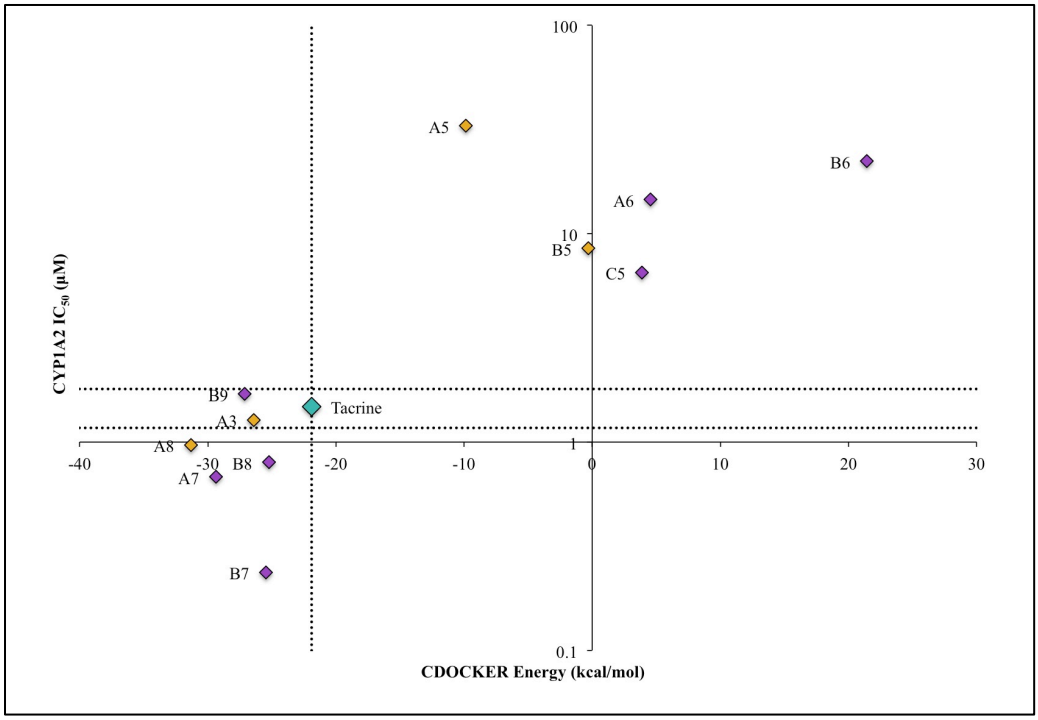

Figure 20. Correlation of *in vitro* CYP1A2 IC_{50} and CDE. *Green*: tacrine; *purple:* eliminated derivatives *yellow:* derivatives for further investigation; *dashed horizontal lines:* standard deviation from n = 3 *in vitro* experiments.

A moderate correlation (R^2 = 0.66963) was observed but it is important to consider that the compounds explored in this study were very structurally similar. Although the software may not be able to distinguish between different nitrogen positions in the

picolyl substituent, it is able to evaluate these compounds' affinity for CYP1A2 relative to tacrine with accuracy.

4.3 Tacrine and its Derivatives as Substrates for P-gp

4.3.1 Determining Clinically Relevant P-glycoprotein Activity

The inward facing conformation of the efflux transporter P-gp consists of 12 helical transmembrane domains (TMDs) two nucleotide-binding domains (NBDs). P-gp has a large internal cavity with a volume of approximately 6000 $Å^3$ and the ability to bind to two molecules simultaneously.[88] The substrate-binding pocket of P-gp is known to be hydrophobic and lies at the interface of TMD6 and TMD12.[89] For these experiments, we used the crystal structure of mouse P-gp bound to the cyclic peptide QZ59-SSS (PDB file: 3G61), as a high-resolution structure of human P-gp has not been reported[90]. Rat P-gp shares 92% sequence identity with mouse P-gp, and shares ~100% identity within the P-gp substrate binding pocket.[91]

The P-gp modelling studies were optimized by using the marketed anti-AD agent donepezil.[92] Analysis of the most stable donepezil-P-gp complex shows that it binds deep in the internal cavity between TM7 and TM12 in a linear conformation. The 5,6-dimethoxyindan-1-one moiety was in van der Waal's contact with the Leu335, Ile336 and Phe339 residues (distances < 5 Å). The benzylpiperidine substituent was oriented in a hydrophobic region comprised of Leu300, Leu720, Phe726, Phe766, Phe833, Val978 and Ala981. The protonated piperidine N*H* underwent a hydrogen bonding interaction with the C=*O* of Gln721 (distance = 1.9 Å), and a π-alkyl interaction was observed between the benzylpiperidine aromatic ring and the isopropyl side chain of Leu300

(distance < 5 Å). A hydrophobic surface map of the donepezil binding region in P-gp indicates that the benyzlpiperidine ring is the major contributing factor in its ability to bind P-gp (EC_{50} = 34.85 ± 4.63 μM). In contrast, a similar modelling study of the antifungal agent ketoconazole shows that it binds in a hydrophobic region between TM6 and TM12, and exhibits better binding affinity (CDIE = -39.27 kcal/mol) and stability (CDE = -20.03 kcal/mol) compared to donepezil (CDIE = -32.94 kcal/mol; CDE = -4.95 kcal/mol). This can be attributed to its ability to interact with a greater number of hydrophobic regions in the substrate-binding pocket (EC_{50} = 9.74 ± 1.23 μM). The acetylpiperazine moiety was oriented toward a hydrophobic region whereas the 2,4-dichlorophenyl ring was in van der Waal's contact with Met68, Phe332, Leu335, Ile336, Phe339 and Tyr949 (distances < 5 Å). In addition, the 2,4-dichlorophenyl aromatic ring underwent an edge-to-face π-π interaction with Phe332 (distance < 5 Å). The C-2 chlorine atom underwent an edge-in Cl-π interaction with Tyr949 aromatic ring (distance < 5.2 Å) whereas the C-4 chlorine underwent hydrophobic interactions with side chains of Met68 and Ile336 (distance < 5 Å). The imidazole aromatic ring formed a π-alkyl interaction with the CH_3 group of Ala981 (distance < 5 Å). The construction of a hydrophobic surface map of the P-gp substrate-binding pocket clearly indicates the ability of ketoconazole to bind to multiple hydrophobic regions. It should also be noted that ketoconazole has a larger molecular volume (407.7 $Å^3$) relative to donepezil (327.7 $Å^3$). These observations explain the superior P-gp inhibition exhibited by ketoconazole (EC_{50} = 9.74 ± 1.23 μM).

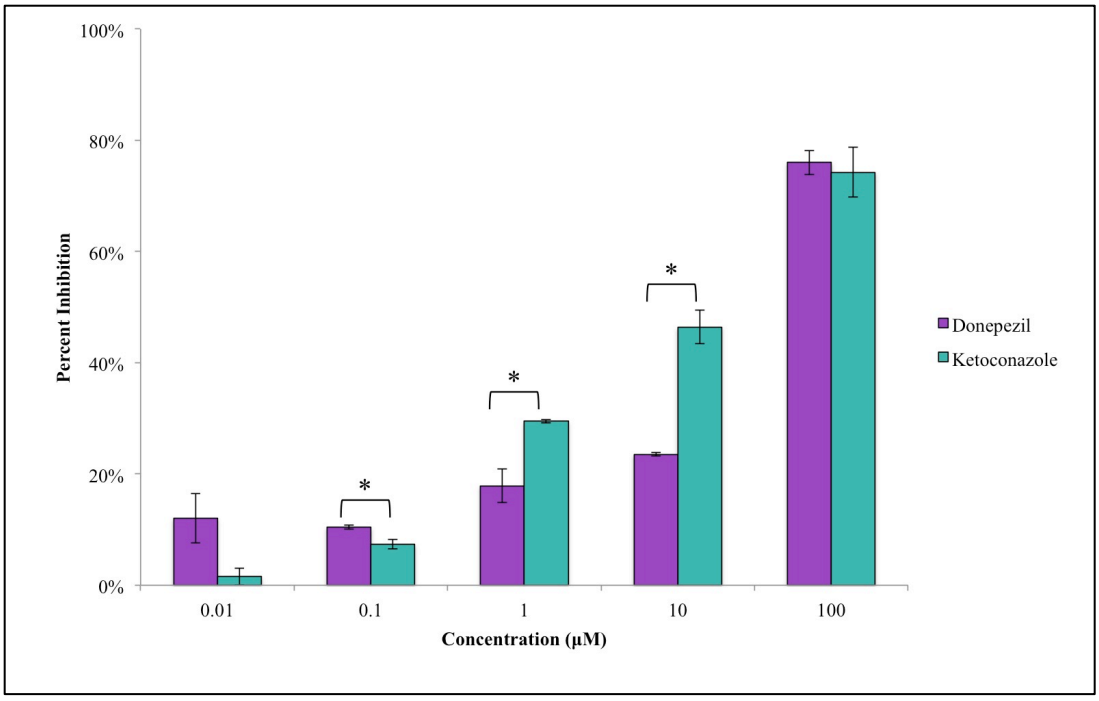

Figure 21. P-gp inhibition profile of donepezil and ketoconazole at increasing concentrations (0.01-100 µM). Results are expressed as % inhibition ± SD (n = 3) for two independent experiments.

Donepezil is a cholinesterase inhibitor that is widely prescribed to improve cognitive decline in AD patients. Literature data suggests that it undergoes liver metabolism primarily through the CYP3A4 enzyme,[93,94] but donepezil's status as a substrate for P-gp. has not been as well characterized; several recent publications disagree on this classification. A number of *in vitro* studies have reported that the efflux ratio for donepezil does not reach the minimum value needed to be considered a P-gp substrate.[95, 96] Ishiwata and co-workers [97] demonstrated that donepezil's brain permeability is compromised due to its interaction with P-gp in the endothelial cells. This

study also showed that the brain-to-blood ratio of radiolabelled donepezil increased significantly in the presence of a P-gp inhibitor. Furthermore, in a porcine *in vitro* blood-brain barrier permeability model, donepezil was shown to be a relatively weak P-gp substrate at a substrate concentration of 3 μM.[98] At unbound plasma concentrations resulting from single or multiple oral donepezil doses of 5 or 10 mg (total steady state concentration for 5 mg = 0.06 μM; unbound fraction = 0.04), it is unlikely that co-administration of donepezil with P-gp inhibitors would result in a clinically significant enhancement of brain permeability.

Other evidence to suggest that *in vivo* therapeutic concentrations, even in the gastrointestinal tract, are in the range of low P-gp inhibition that we determined in our study is the excellent oral bioavailability of donepezil (around 92%).[99] Intestinal P-gp efflux of substrates tends to promote its metabolism by CYP3A4 due to the interplay between at the apical intestinal membrane.[100] Some drugs, such as ketoconazole, are known to exhibit high affinity for CYP3A4 and P-gp, which can manifest in low oral bioavailability (absolute bioavailability in dogs is 50%; no human IV formulation).[101] The high oral bioavailability of donepezil confirms its low P-gp affinity.

In conclusion, molecular modelling investigations of donepezil and P-gp indicate that interactions with the hydrophobic regions of the P-gp substrate-binding pocket contribute substantially to the stability of the complex. When compared to ketoconazole, donepezil undergoes fewer of these desirable interactions and displays a lower affinity for P-gp. The results of the *in vitro* P-gp assay corroborate this finding, indicating that donepezil is a weak substrate for P-gp at clinically relevant concentrations. Our study suggests that neither the co-administration of donepezil of P-gp inhibitors to enhance

brain permeability nor the concomitant use of other P-gp substrates is expected to result in clinically significant drug interactions.

4.3.2 Evaluating Tacrine and its Derivatives as P-glycoprotein Substrates

Tacrine's relationship with P-gp has been less controversial than that of donepezil. Several studies have determined *in vitro* that tacrine has an efflux ratio of approximately 1, indicating that its entry into the CNS is not modulated by P-gp.[102,103] Rather, it has been observed in rat brain that organic cation transporter (OCT) systems are likely involved in the transport of tacrine across the BBB.[81] The most stable conformation of tacrine within the P-gp drug-binding site shows the tetrahydroacridine ring system in the same hydrophobic region as the benzylpiperidine and acetylpiperazine groups of donepezil and ketoconazole, respectively. As a result, tacrine undergoes some similar interactions with Val978 (hydrogen bond, 2.7 Å) and Ala981 (π-alkyl interaction, 4.7 Å), found on TMD12. Additionally, π-amide stacking occurs between the Ala981-Met982 peptide bond and the π-orbitals of tacrine (4.1 Å). However, tacrine is unable to form interactions with other TMDs as observed with donepezil (CDIE = -32.94 kcal/mol) and ketoconazole (CDIE = -39.27 kcal/mol) due to its smaller size and more isotropic shape and thus exhibits lower affinity for P-gp (CDIE = -20.57 kcal/mol). The stability of the tacrine-P-gp complex (CDE = -7.12 kcal/mol) is also considerably lower than that of ketoconazole (CDE = -20.03 kcal/mol) and similar to that of donepezil (CDE = -4.95 kcal/mol). From these results, it is anticipated that tacrine would have a high EC_{50} for P-gp and the *in vitro* P-gp assays confirm this (EC_{50}: 348 ± 27.3 μM).

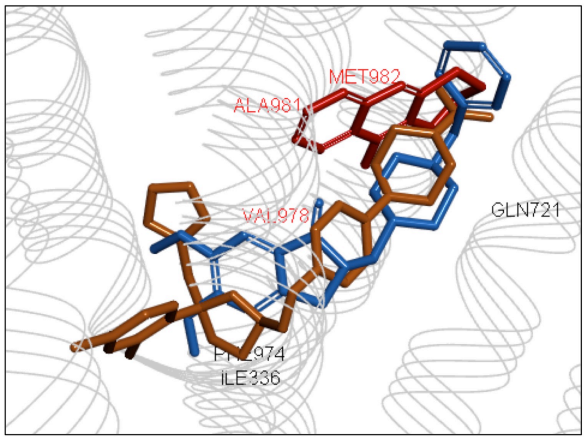

Figure 22. Comparison of tacrine (red), donepezil (blue) and ketoconazole (orange) positioning within the P-gp substrate binding site.

It was hypothesized that the tacrine derivatives may display enhanced P-gp binding due to their larger size (molecular volume range: 203.4 – 260.3 Å^3) compared to tacrine (139.9 Å^3). Generally, the tetrahydroacridine ring is situated in the same location as tacrine and also undergoes interactions with Val978 and Ala981, and the large C-9 substituent is able interact with additional residues that were too distant from tacrine. This is reflected in the CDIEs of the tacrine derivatives (-25.28 to -31.99 kcal/mol; tacrine: -20.57 kcal/mol). Three out of four tacrine derivatives underwent close hydrogen bonding interactions with Gln721 (distance < 2.5 Å), which was also observed for donepezil and for the co-crystallized ligand QZ59-SSS[104]. This residue was reported to be the most common site for hydrogen bonding, despite the presence several other residues capable of hydrogen bonding in the drug-binding pocket.[105] Although they undergo a greater number of interactions, the complexes formed between P-gp and the tacrine derivatives are not very stable; the CDE parameter varied between -6.80 kcal/mol

and -8.97 kcal/mol. CDE appears to be more correlated with P-gp activity than CDIE, as ketoconazole and donepezil have quite different P-gp EC_{50}'s and differ more in CDE (difference of 15.08 kcal/mol, compared to a difference of 6.33 kcal/mol for CDIE).

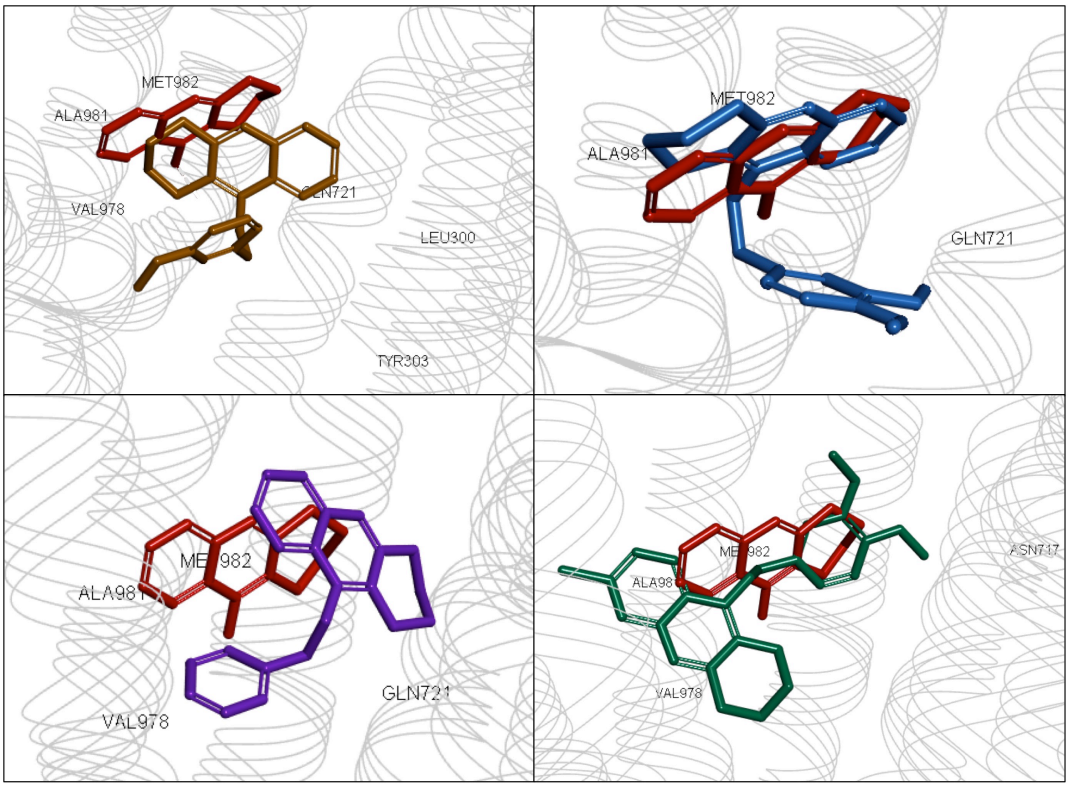

Figure 23. Orientation of tacrine and derivatives within the P-gp substrate binding site. *Red:* tacrine; *orange:* A3; *blue*: A5; *purple:* A8; *green:* B5.

The *in vitro* assays support the hypothesis that additional substituents at the C-9 position will increase the likelihood of P-gp binding. The tacrine derivatives displayed EC_{50} values that are significantly lower than tacrine (EC_{50} range: 52.4 ± 5.9 μM – 72.4 ± 10.5 μM). Although these represent a significant change from tacrine, the derivatives still exhibit far less activity towards P-gp than donepezil. As a result, P-gp is not expected to have a noticeable impact on the PK profile of tacrine and its derivatives.

4.4 Evaluating Tacrine and its Derivatives as CYP3A4 Substrates

CYP3A4 is considered to be the most important enzyme in drug metabolism. It is estimated to have a role in the metabolism of 60% of all clinically used drugs and is frequently the cause of drug-drug interactions (DDIs).[106] The prediction of DDIs in early phases of drug development has recently become a priority as several drugs have been removed from the US market due to DDI-related safety concerns.[107] For these reasons, it is important to investigate the interactions of any candidate molecule with CYP3A4. For this study in particular, interaction with CYP3A4 must be explored for a second reason. Although CYP1A2 is the primary enzyme involved in the metabolism of tacrine, all members of the CYP450 family can catalyze oxidation reactions, so metabolism by any CYP isozyme may produce unwanted metabolites. Compounds A3, A5, A8 and B5 are oriented in a favourable position within the CYP1A2 active site but the binding site for CYP3A4 is considerably larger than that of CYP1A2 (1385 $Å^3$ and 375 $Å^3$, respectively[31]), and increases further upon ligand binding (1500-2000 $Å^3$, Figure 24).[108] The additional volume may allow for different binding modes for these compounds and subsequent formation of toxic species.

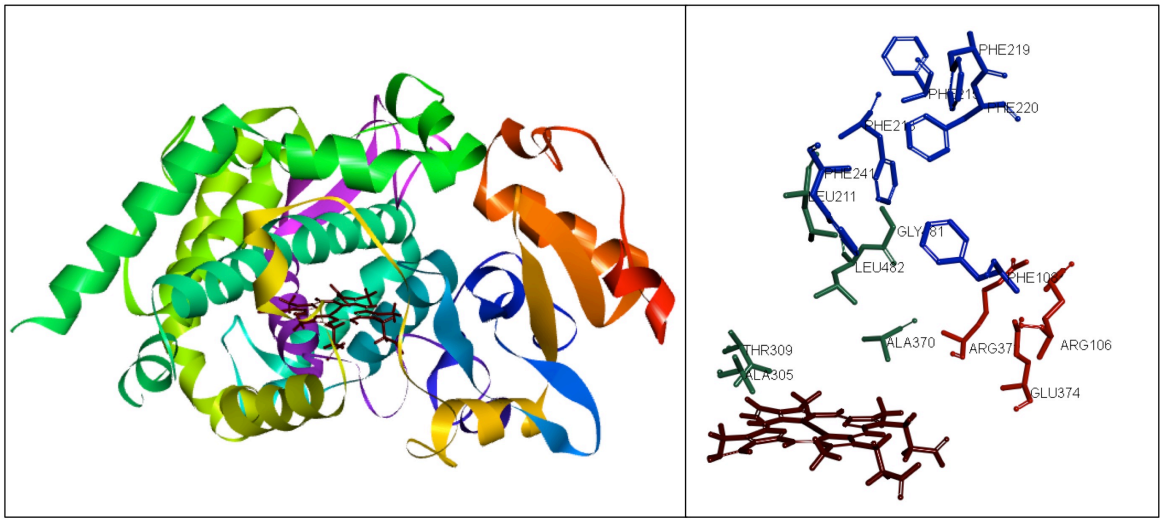

Figure 24. Left: 3D structure of the CYP3A4 enzyme (PDB file name: 2V0M). Right: CYP3A4 active site. *Blue:* phenylalanine cluster; *red*: keto group; *green:* key binding residues; *dark red:* heme prosthetic group.

The CYP3A4 docking protocol was validated by docking the known ligand ketoconazole.[92] Compound interactions with CYP3A4 were evaluated using the same techniques as the analogous studies with CYP1A2. As with the CYP1A2 study, any compounds oriented with the tetrahydroacridine ring closest to the heme group were eliminated. Of the four compounds docked, only one was eliminated based on the above criteria. A3 was unfavourably positioned in the two most stable complexes, and in four of the ten poses overall (Figure 25).

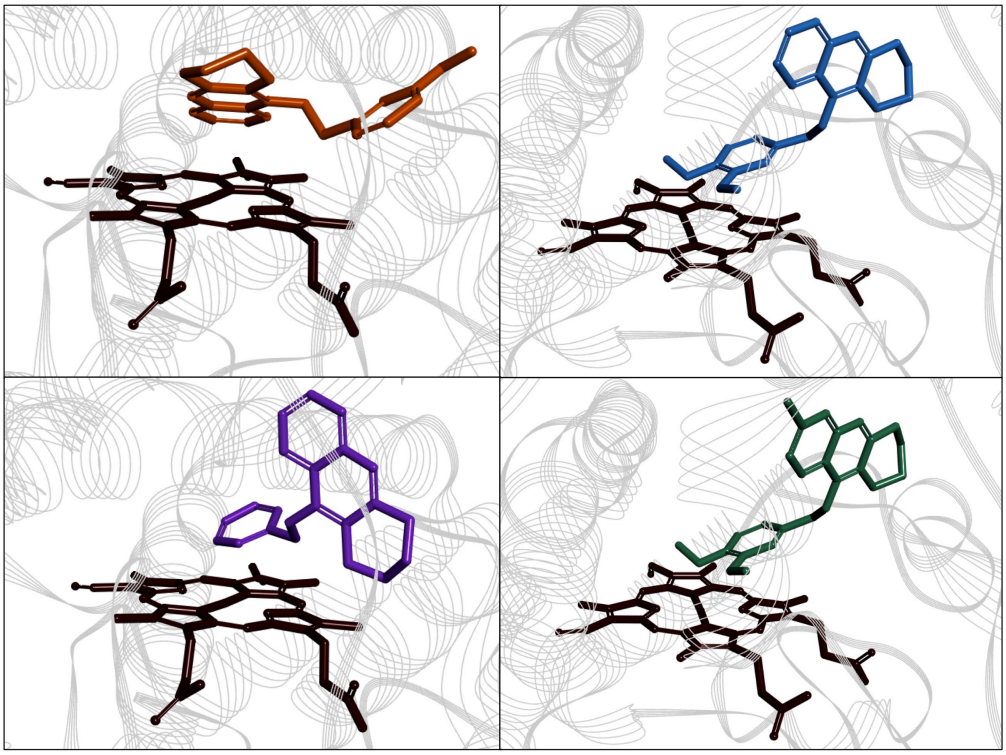

Figure 25. Orientation of tacrine derivatives within the CYP3A4 site. *Dark red:* heme prosthetic group; *orange:* A3; *blue*: A5; *purple:* A8; *green:* B5.

Compounds A5 and B5 formed significantly more stable complexes with CYP3A4 as compared to CYP1A2 (CDE decreased by 10 and 21 kcal/mol, respectively). Since the CDIEs are approximately the same for both enzymes (approximately -45 kcal/mol for both compounds, for both enzymes), the increased stability is likely due to the larger volume of the active site. Another common observation for both of the 3,4-dimthoxybenzyl-substitued compounds is the formation of a close carbon hydrogen bond between a methyl hydrogen on the 4-methoxy group and the hydroxyl oxygen of residue Thr309 (distances < 2.3 Å), which encourages the molecule to dock with the C-9 group closest to the heme. The increased stability of the complex was more apparent for

compound A5 compared to B5. For A5, IC_{50} decreased by a factor of 10 (CYP1A2 IC_{50}: 33.0 ± 2.7 μM; CYP3A4 IC_{50}: 3.7 ± 0.4 μM). Conversely, there was no significant difference between the B5's IC_{50} for CYP1A2 and CYP3A4 (8.5 ± 1.5 μM and 13.8 ± 1.1 μM, respectively).

Compound A8, which contains a 3-picolylamine substituent, displayed notably lower affinity for CYP3A4 than CYP1A2, despite the presence of three close interactions with residues Arg372 and Glu374 in the keto pocket (distances < 2.5 Å). This trend was also observed in the *in vitro* studies, as A8's IC_{50} for CYP3A4 was 9.1 ± 1.1 μM compared to 1.0 ± 0.5 μM for CYP1A2. The overall orientation of A8 with respect to the heme group is similar to that observed in CYP1A2, and it is likely that the coordinate covalent bond between the picolyl nitrogen and the heme iron atoms described earlier also forms within the CYP3A4 binding pocket.

4.5 Isolation and Characterization of Rat Liver Microsomes

Livers were obtained from three male Sprague-Dawley rats and weighed 7.45 g, 12.95 g and 10.8 g for Rat #1, Rat #2 and Rat #3, respectively. Many different test systems exist for the investigation of metabolism kinetics. Hepatocytes offer the best recreation of the *in vivo* environment, as they contain both the CYP450s and phase II enzymes such as glutathione, sulfatases and S-transferases. However, their preparation is more complicated. Since the CYP450 enzymes are almost entirely responsible for the metabolism of tacrine, microsomes – the subcellular fraction containing the endoplasmic reticulum – are a suitable representation, and are simpler to isolate and more stable during storage.

The protein content and cytochrome P450 reductase (CPR) activity of the microsomes were then quantified using the Bradford protein assay and a ferricyanide-based assay, respectively. The protein content was 38.50, 36.22 and 32.41 mg of microsomal protein per gram of liver (MPPGL) for Rat #1, Rat #2 and Rat #3, respectively. These values are close to the 45 MPPGL often cited in the literature[109] and correspond to a recovery rate of 72.0-85.6%. The reduction rate of ferricyanide was found to be 60.64, 27.11 and 25.35 mM per minute per milligram of microsomal protein.

Table 3. Properties of isolated microsomes.

Rat	Liver Weight (g)	MPPGL (mg/g)	Recovery Rate	Reduction Rate (mmol/L/min/mg)
1	7.45	38.50	85.56%	60.64
2	12.95	36.22	80.49%	27.11
3	10.80	32.41	72.02%	25.35

4.6 Measurement of *In Vitro* Intrinsic Clearance

4.6.1 Substrate Depletion Studies

Traditionally, enzyme kinetic parameters are evaluated by observing the rates of product formation at several different substrate concentrations. This method requires definitively identified metabolic pathways, but knowledge of such pathways and metabolites is often lacking in the early stages of drug development. In this scenario, the substrate depletion approach, in which the consumption of substrate is monitored over

time at multiple substrate concentrations, is a more practical approach.[110] Furthermore, the substrate depletion method, proposed by Obach and Reed-Hagen in 2002,[111] has been shown to be equivalent to the more traditional product formation approach.[112]

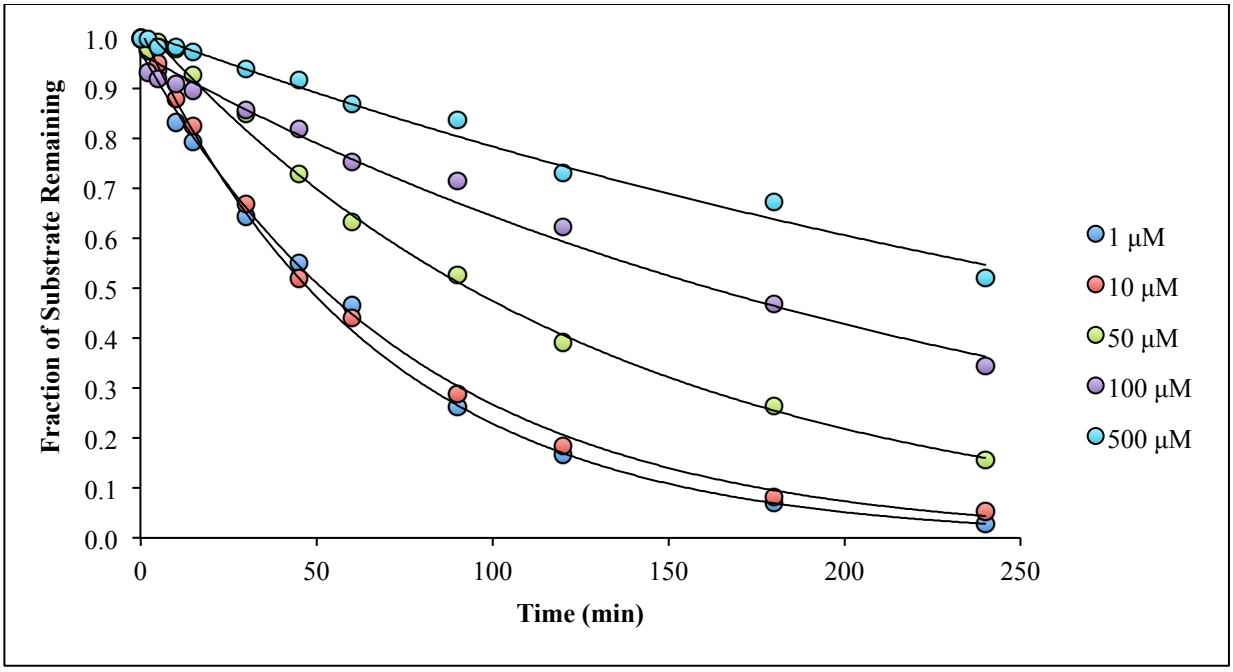

Figure 26. Depletion of tacrine over time at various concentrations.

Each of the curves in Figure 26 was fit to a single exponential to determine the depletion rate constant for each concentration. A plot of rate constant versus concentration was then produced and $k_{dep([S]\rightarrow 0)}$ and K_m were extracted.

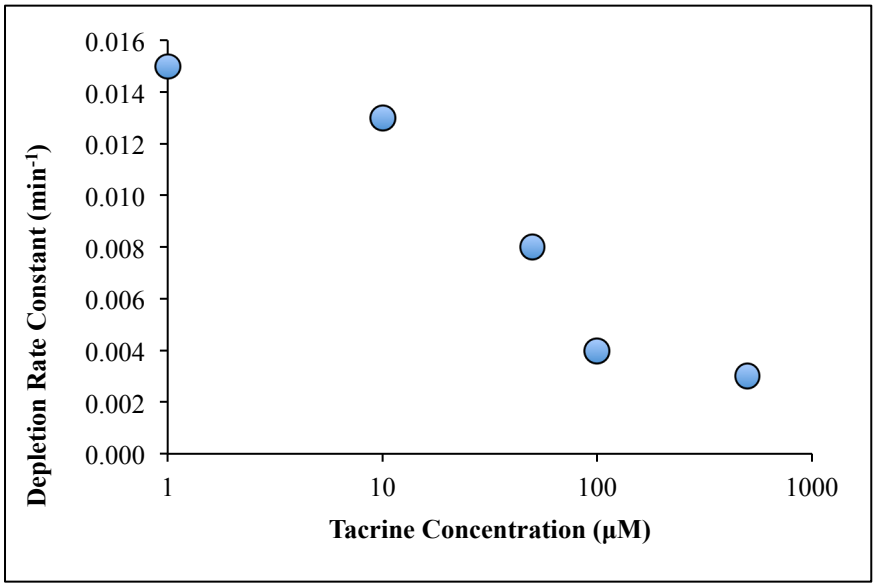

Figure 27. Plot of *in vitro* depletion rate constant versus tacrine concentration.

The data in Figure 27 was fit to the following curve to obtain estimates of the depletion rate constant and the Michaelis constant:

$$k_{dep} = k_{dep([S]\rightarrow 0)}\left(1 - \frac{[S]}{[S] + K_m}\right)$$

$$k_{dep} = 0.015\ min^{-1}\left(1 - \frac{[S]}{[S] + 49.3\ \mu M}\right)$$

The K_m derived from this experiment (49.3 µM) was considerably greater than that reported by Obach and Reed-Hagen (1.4 µM). This is likely due to the fact that Obach and Reed-Hagen used recombinant human CYP1A2 microsomes at a concentration of 0.92 mg/mL. Although the concentration used in this project was greater, these microsomes are not isozyme-specific and only contain the naturally occurring concentration of CYP1A2.[112] Kinetic parameters for tacrine derivatives are shown in Table 5.

4.6.2 Microsomal Binding Assays

Fraction unbound in microsomal protein was determined using microdialysis. The microdialysis set-up consists of two chambers separated by a membrane with pores such that the free ligand can cross the membrane but the receptor-bound ligand cannot. The ligand continues to diffuse across the membrane until the unbound concentrations on either side of the membrane are equal.

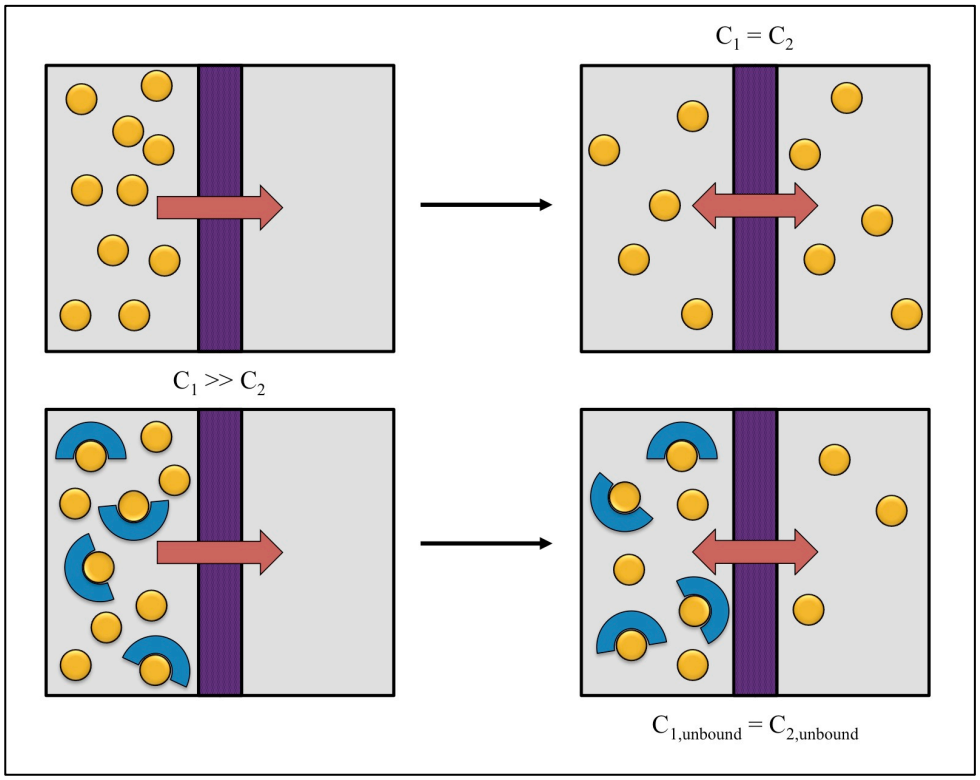

Figure 28. Principle of microdialysis. Top: When protein binding does not occur, total ligand concentration on either side of the diffusion membrane are equal. Bottom: If protein binding occurs, unbound concentrations are equal but the total concentration is greater in the chamber containing the protein.

Other methods for determining fraction unbound include equilibrium dialysis, ultrafiltration and ultracentrifugation. Equilibrium dialysis is typically considered to be the gold standard for protein binding studies. Both equilibrium dialysis and microdialysis use the same principle, but the smaller sample size used in microdialysis requires a shorter dialysis time, thereby reducing the likelihood of drug and/or protein degradation and microbial growth.[113] The agreement between microdialysis and equilibrium dialysis has been studied extensively[114,115]; Le Quellec and coworkers found a correlation factor of r = 0.96 for samples from rabbit, rat, monkey and human.[116]

In the same way that drug bound to plasma proteins is unavailable to target tissues, drug that is bound to microsomal protein is assumed to be inaccessible to metabolizing enzymes. Overlooking nonspecific microsomal binding can significantly hinder predictions of *in vivo* clearance.[117,118] Bases are particularly prone to high degrees of microsomal binding, and a strong correlation between lipophilicity and extent of binding has been observed at a protein concentration of 1 mg/mL[119]:

$$log\left(\frac{1-f_{u,mic}}{f_{u,mic}}\right) = 0.53logP - 1.42$$

Given this trend, nonspecific binding to microsomal protein was expected to be a major factor in predicting clearance for tacrine and its derivatives.

Table 4. Fraction unbound in microsomal incubations

Compound	λ_{max}	$f_{u,mic}$
Tacrine	320 nm	0.012
A5	340 nm	0.011
A8	340 nm	0.010
B5	270 nm	0.035

4.6.3 Physiologically Based Scaling of *In Vitro* Intrinsic Clearance

In order to estimate the intrinsic clearance of the whole liver from *in vitro* kinetic parameters, a scaling factor (SF) must be applied. The SF must account for the amount of protein present in the incubation, the protein concentration in the liver, and the total size of the liver.

$$CL_{int} = k_{dep([S]\rightarrow 0)} \times \frac{1}{f_{u,mic}} \times \frac{mL\ incubation}{mg\ microsomes} \times \frac{mg\ microsomes}{g\ liver} \times g\ liver$$

The first two terms in the scaling factor incorporates the fraction unbound in microsomes and the protein concentration for the incubation (2 mg/mL). The final two terms are known values from the literature. The average microsomal protein per gram of liver (MPPGL) for rat is 45 mg/g.[120] A moderate correlation between rat liver weight and body weight has also been observed:[121]

$$\%LW = 5.92 - 0.00286\ BW$$

where %LW is the liver weight as a percentage of body weight. From this relationship, a rat with a body weight of 400 g would have liver that weighs 4.776% of its total body weight, or 19.1 g. Plugging these three values into the equation above produces the following relationship:

$$CL_{int} = \frac{429.75}{f_{u,mic}} k_{dep([S]\rightarrow 0)}$$

where CL_{int} has units of mL/min.

Table 5. Kinetic parameters from substrate depletion studies and scaled estimates of *in vitro* intrinsic clearance.

Compound	$k_{dep([S]\rightarrow 0)}$	K_m	$f_{u,mic}$	$CL_{int,s}$
Tacrine	0.015 min^{-1}	49.3 μM	0.012	537 mL/min
A5	0.013 min^{-1}	48.1 μM	0.011	508 mL/min
A8	0.015 min^{-1}	55.5 μM	0.010	645 mL/min
B5	0.011 min^{-1}	52.1 μM	0.035	135 mL/min

It is important to note that the physiologically based approach for scaling *in vitro* CL_{int} has been shown to systematically underpredict *in vivo* CL_{int}, and this bias cannot be corrected without *in vivo* data.[122] For tacrine, the optimized minimum CL_{int} was 700 mL/min. However, upon optimizing the PBPK model, it became apparent that hepatic clearance was blood flow limited and that direct scaling of the values in Table was not directly translatable even in the presence of observed data. Nevertheless, the relative values between tacrine and its derivatives could provide valuable information for parameterization, as discussed in the next section.

4.7 Development of PBPK Models for Tacrine and Derivatives

4.7.1 Choice of Model Animal

PBPK models of tacrine and its derivatives were developed for rats for several reasons. First, rat physiology is better characterized than mouse physiology, and is also more human-like.[123] A number of studies have examined the ability of the rat to reflect human responses to various stimuli, and the differences between the rat and human reactions are often insignificant.[124,125] Rats are also much larger than mice, allowing for larger sample volumes, easier surgeries and higher resolution imaging in preclinical studies. Additionally, several rat models of Alzheimer's disease have been developed in recent years using both transgenic and non-transgenic rats. These rats display amyloidosis, hyperphosphorylated tau and neuronal loss in the cerebral cortex and hippocampus.[126,127] Because they are both more social and more intelligent than mice, the behavioural changes and cognitive impairment associated with Alzheimer's disease can be observed more easily in rat models; this well-defined behaviour can be extremely useful in accurately assessing cognition.[128]

4.7.2 Parameterization of Tacrine Model

The initial tacrine model was parameterized using data from several literature sources, including plasma protein binding data and dosing protocol from Telting-Diaz and Lunte[81], physicochemical properties from Goh et al.[129] and pK_a from Perrin[130] (Table 4).

Table 6. Physicochemical input parameters for the rat IV tacrine model.

Parameter	Value	Reference
Molecular Weight (g/mol)	198.27	Goh et al., 2010
ClogP	3.27	Goh et al., 2010
pKa	9.95	Perrin, 1972
B:P	1.64	Telting-Diaz and Lunte, 1993
Fraction Unbound	0.438	Telting-Diaz and Lunte, 1993

Originally, the model was parameterized with no transporter activity at the blood-brain barrier. If brain concentrations were overpredicted, then the P-gp data that was collected *in vitro* would be integrated into the model. *In silico* and *in vitro* experiments, as well as previous studies found in the literature, suggested the P-gp would not be a major determinant in tacrine's disposition. The results of the first simulation indicated that the model was in fact underpredicting brain concentration, and so tacrine transport by P-gp was deemed negligible. In order to achieve the brain concentrations observed in the Telting-Diaz study, an influx transporter into the brain was incorporated. The most common uptake transporters are the solute carrier (SLC) family of proteins. Like P-gp, the SLC family of proteins consist of 12 TMDs but little is known about how substrates interact with this family of proteins. There are more than 300 members in the SLC family, which are further divided in 52 sub-groups including transporters for urea, amino acids and acetyl-CoA.[131] Since tacrine is protonated at physiological pH, the increased

uptake observed in the *in vivo* study is likely due to a member of the organic cation transporter (OCT) group. The OCT family contains at least five distinct members: OCT1, OCT2, OCT3, OCTN1 and OCTN2. Sung and coworkers determined which members of the OCT family are present in the BBB of rat brain samples and tacrine's affinity for each one.[84] It was determined that only OCT2 and OCTN2 are localized in the BBB of rats, and that tacrine has a much higher affinity for OCT2 as compared to OCTN2, with an estimated K_M in the low micromolar range.[80]

Table 7. Optimized parameters for the rat IV tacrine model.

Parameter	Initial Value	Final Value
CYP1A2 CL_{int} (L/min)	1.0	0.7
Brain Permeability (cm/min)	0.4447	0.003
$K_{p,brain}$[a]	3.4912	3.4912
OCT2 V_{max} (μmol/mL/min)	0	1.0
P-gp V_{max} (μmol/mL/min)	0	0

[a]Accumulation due to passive transport as defined using Rodgers and Rowland algorithms for prediction of organ:plasma partition coefficients.[132]

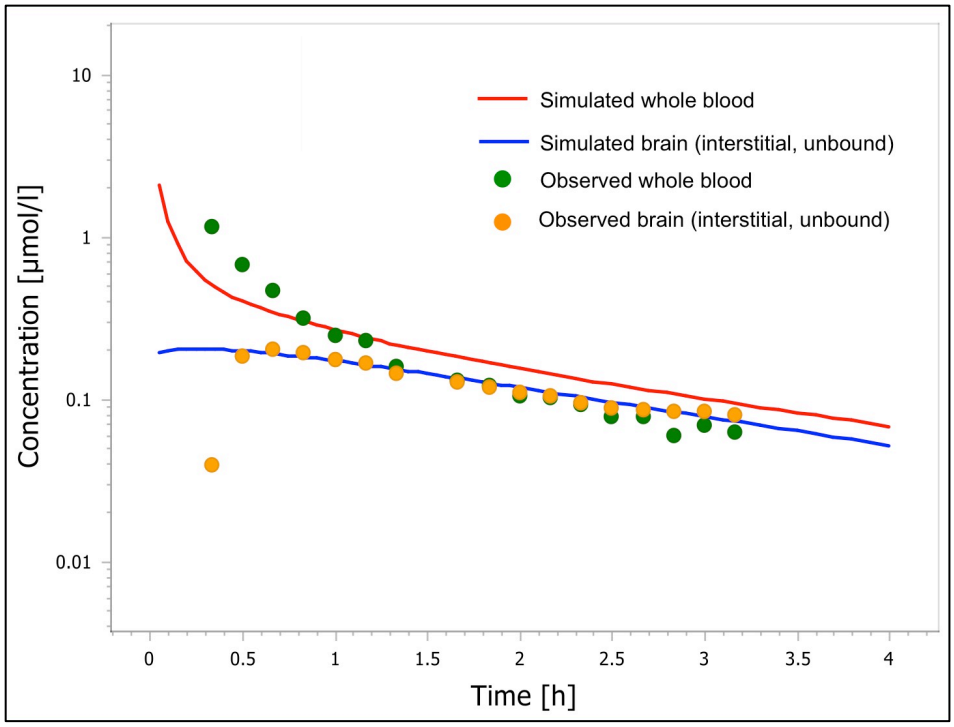

Figure 29. Simulated (lines) and observed (dots) concentration-time data for tacrine following a 1 mg/kg IV bolus administration.

4.7.3 Parameterization of Tacrine Derivative Models

Since brain permeability was overpredicted in the tacrine model, this parameter was also modified in the models for the tacrine derivatives. The new value for permeability was obtained by multiplying by the ratio of optimal to estimated brain permeability for tacrine.

$$permeability\ scaling\ factor = \frac{optimal}{estimated} = \frac{0.003\ cm/min}{0.4447\ cm/min} = 0.00675$$

Although tacrine is a known substrate for OCT2, it is unknown how the derivatives would interact with this protein. As mentioned, little is known about this

family of transporters, including their 3D structure. As a result, molecular docking experiments were not an option for predicting substrate behaviour. However, a pharmacophore modelling approach has been employed by a number of groups and several indicators of OCT2 substrate behaviour have been explored. These include molecular volume, polar surface area, $logD_{7.4}$,[133] aromaticity, ionization,[134] logP and molecular shape.[135]

Table 8. Properties determining OCT2 substrate behaviour and how these properties differ between tacrine and its derivatives

Study	Property	Effect on Transport[a]	Tacrine	A5	A8	B5
Hendrickx et al. (2013)[127]	Molecular volume	↓	139.9 $Å^3$	249.4 $Å^3$	201.0 $Å^3$	260.3 $Å^3$
	Polar surface area	↓	38.90 $Å^2$	43.4 $Å^2$	37.8 $Å^2$	43.4 $Å^2$
	$logD_{7.4}$	↑	2.02	4.05	2.89	4.75
Xu et al. (2013)[128]	Aromaticity	↑	✔	✔	✔	✔
	Positive charge	↑	+1	0	+1	0
Suhre et al. (2005)[129]	logP	↑	3.27	5.18	4.02	5.99
	Length of molecule	No effect	n/a	n/a	n/a	n/a

. [a] An arrow pointing up (down) indicates a positive (negative) correlation between OCT2 transport and the corresponding property.

In many cases, the tacrine derivatives display properties that are equally or more favourable for OCT2 transport than tacrine. The most likely attribute to decrease transport by OCT2 is their size, which is significantly greater than tacrine (44-86% larger). However, the study by Suhre and coworkers examined a range of structurally diverse organic cations, many of which are similar to compounds A5, A8 and B5 in terms of size. For example, the crystal of violet dye, which has a molecular weight of 407.98 g/mol, has IC_{50} values of 2.6 ± 1.2 μM in human OCT2 and 2.05 ± 0.2 μM in rabbit OCT2. For this reason, it was predicted that size would not impede the transport of tacrine derivatives by OCT2 and they were parameterized using the same values as tacrine.

PBPK models were developed for each derivative using the same rat-specific inputs (e.g. organ volumes and blood flows) as were used for tacrine. The input parameters relating to each derivative are presented in Table 7. A final rat PBPK model following IV administration of 1 mg/kg was created for A5, A8 and B5.

Table 9. Summary of tacrine derivative-specific parameters for the rat IV PBPK models.

	Value			
Parameter	A5	A8	B5	Source
Molecular Weight (g/mol)	348.42	289.38	382.88	Mass spectrometry
Halogens present?	None	None	1 Cl	Chemical structure
ClogP[a]	5.18	4.02	5.99	ChemDraw
pKa[a]	8.5	8.5	8.61	Discovery Studio 4.0
$CL_{int,s}$ (L/min)	0.7	0.7	0.7	Substrate depletion studies and tacrine model
Glomerular Filtration	Yes	Yes	Yes	Tacrine model
P-gp V_{max} (µmol/mL/min)	0	0	0	*In vitro* assays and *in silico* molecular docking
OCT2 V_{max} (µmol/mL/min)	1.0	1.0	1.0	Pharmacophore modelling
Brain Permeability (cm/min)	0.0082	0.0017	0.04226	Scaled based on tacrine model

4.7.4 Dosing Guidelines for Preclinical Studies

In order for a drug to be effective, it must be present in a sufficiently high concentration at the site of action. In the case of the tacrine derivatives, the site of action is the brain intracellular space and the desired concentration will depend on each compound's ability to inhibit AChE activity by 90% (IC_{90}). To assess the dose needed to reach these concentrations, a multiple dose protocol was simulated for each compound

consisting of a 1 mg/kg dose given every 6 hours for 600 hours, such that all compounds had reached steady state in the brain. The average unbound, intracellular brain steady state concentration (C_{ss}) was determined for the 1 mg/kg dose (Table 8). Because of the non-linear aspects of the OCT2 transporter with a K_m value on par with blood concentrations, dose could not be scaled linearly from the 1 mg/kg simulation. As a result, the dose was manually adjusted until C_{ss} reached AChE IC_{90}.

Table 10. Necessary IV dose to reach AChE IC_{90} in the brain intracellular space (unbound).

	C_{ss} for 1 mg/kg dose (µM)		**AChE IC_{90} (µM)**	**Necessary Dose (mg/kg)**
Compound	**Brain intracellular space**	**Blood**		
Tacrine	0.1	0.4	1.75	17.5
A5	0.5	0.2	13.26	80
A8	2.5	0.2	31.01	28
B5	0.1	0.1	9.05	180

From the above table, it is clear that compound A8 is able to accumulate in the brain to a much greater extent than the other molecules, including tacrine. As shown in Table 7, A8 has the lowest passive BBB permeability, but this permeability is bidirectional (i.e. A8 will both enter and leave the brain at the slowest rate). The slow passive diffusion into the brain is overcome by OCT2 transport, allowing for a steady increase in concentration and a lower dose needed to reach IC_{90}.

Chapter 5.0 Conclusions and Future Studies

This project serves as a template for the further investigation of tacrine-based compounds for the treatment of AD. In summary, a library of multifunctional tacrine derivatives was further analyzed to determine which candidates are most likely to be successful in later stages of drug development. Existing data was used to single out molecules with potent AChE inhibition and to eliminate compounds that are likely to display undesirable PK due to high lipophilicity. To reduce the risk of hepatotoxicity, compounds were investigated using *in vitro* and *in silico* methods to assess their binding interactions with both CYP1A2, the primary enzyme in tacrine metabolism, and CYP3A4, the most common enzyme for drug metabolism. From molecular docking studies, it is clear that the issue of hepatotoxicity cannot be solved for tacrine simply by adding a large substituent at the C-9 position; the type and size of the substituent will both influence the binding mode within the CYP active site and dictate the site of metabolism. For this reason, molecular docking studies are a crucial step in compound development. Molecules that were predicted to produce nontoxic metabolites were then assessed for substrate behaviour toward P-gp. *In silico* and *in vitro* studies agreed with the literature data suggesting that tacrine does not undergo transport by P-gp. The derivatives displayed somewhat enhanced binding properties towards P-gp as compared to tacrine, but showed less P-gp activity than donepezil. As a result, lack of brain permeability due to efflux by P-gp is not a concern for this group of compounds. Substrate depletion studies were conducted to evaluate metabolic stability and derive intrinsic clearances. The process of selecting compounds is illustrated in Figure 29. The *in vitro* and *in silico* data described above were then incorporated into a PBPK model to

predict the dose needed to reach each compound's IC_{90} in the brain as a guide for future preclinical studies.

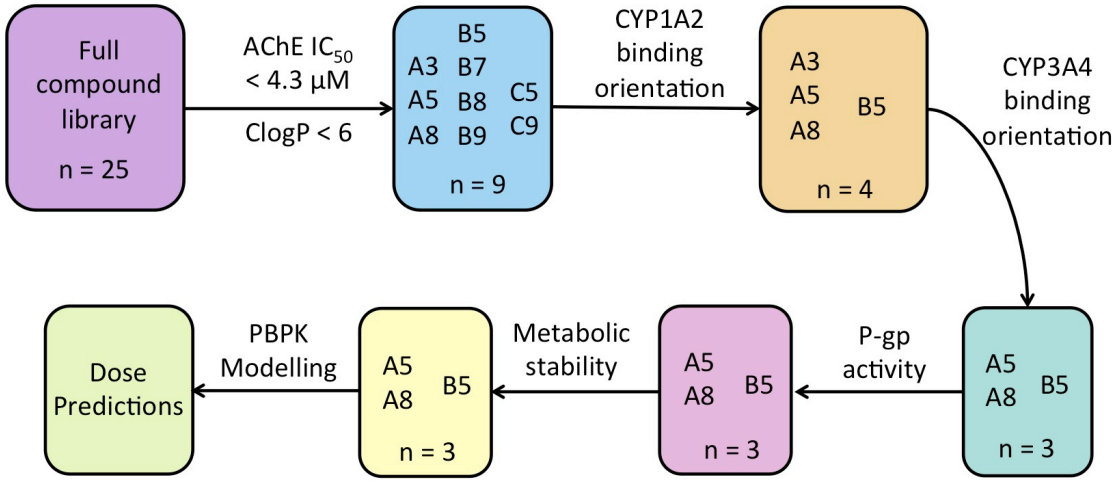

Figure 30. Process of eliminating compounds to identify lead candidates for *in vivo* preclinical studies.

As shown in Figure 29 only 3 compounds displayed all of the desired characteristics based on the *in vitro* and *in silico* experiments. These characteristics are summarized below in Table 9.

Table 11. Summary of characteristics for modeled compounds.

		Compound		
		A5	**A8**	**B5**
CYP1A2	Favourable binding orientation?	✔	✔	✔
	CDOCKER Energy (kcal/mol)	-9.844	-31.32	-0.305
	IC_{50} (μM)	33.0 ± 2.7	1.0 ± 0.5	8.5 ± 1.5
P-gp	CDOCKER Energy (kcal/mol)	-6.799	-7.396	-8.866
	IC_{50} (μM)	63.5 ± 7.1	72.4 ± 10.5	52.4 ± 5.9
CYP3A4	Favourable binding orientation?	✔	✔	✔
	CDOCKER Energy (kcal/mol)	-20.394	-19.806	-21.739
	IC_{50} (μM)	3.7 ± 0.4	9.1 ± 0.7	13.8± 1.1
Additional Information	Cell Viability (25 μM)	93.8%	100.0%	81.8%
	Dose to Reach IC_{90} (mg/kg)	80	28	180

Considering all of the areas investigated, compound A8 appears to be the most promising candidate for further studies. It is the least lipophilic of all compounds investigated (ClogP = 4.02) and, as a result, is less likely to produce unwanted side effects. Its toxicity has been investigated *in vitro*, and cell viability was 100% and 82.1% at concentrations of 25 and 50 μM, respectively. The coordinate covalent bond formed between the picolyl nitrogen and heme iron anchors the molecule in a favourable binding position for both CYP1A2 and CYP3A4, likely preventing the formation of toxic

metabolites. It also displays the most favourable PK profile, requiring the lowest dose to maintain therapeutic concentrations in the brain, despite being the least potent AChE inhibitor of the remaining candidates. For these reasons, A8 is the compound that most warrants further investigation *in vivo*. Prior to these *in vivo* studies, the ability of A8 to inhibit the aggregation Aβ protein should be investigated, as no experiments of this kind have been conducted for a picolyl-substituted compound.

In addition to *in vivo* PK studies guided by the dosing recommendations above, the metabolic profiles of the tacrine derivatives can be further elucidated by conducting substrate depletion studies in the presence of inhibitors of specific CYP450 isozymes such as α-naphthoflavone for CYP1A2 and ketoconazole for CYP3A4. Further confirmation of metabolite structure is also possible through further analysis by LC-MS, for more certain validation that hydroxytacrine metabolites are not being formed in an appreciable amount.

References

1. Goedert, M. and Spillantini, M. G. A century of Alzheimer's disease. *Science*. **2006**, *314*, 777-781.

2. Brookmeyer, R.; Gray, S. and Kawas, C. Projections of Alzheimer's disease in the United States and the public health impact of delaying disease onset. *Am. J. Public Health*. **1998**, *88*, 1337-1342.

3. A new way of looking at the impact of dementia in Canada. Alzheimer Society, 2012.

4. Brookmeyer, R.; Johnson, E.; Ziegler-Graham K. and Arrighi, H. M. Forecasting the global burden of Alzheimer's disease. *Alzheimers Dement*. **2007**, *3*, 186-191.

5. Wilcock, G. K.; Esiri, M. M.; Bowem, D. M. and Smith, C. C. T. Alzheimer's disease: correlation with cortical CAT activity with the severity of dementia and histological abnormalities. *J. Neurol. Sci.* **1982**, *57*, 407-417.

6. Davies, A. P. and Moloney, A. J. F. Selective loss of cholinergic neurons in Alzheimer's disease. *Lancet*. **1976**, *2*, 1403-1404.

7. Hyman, B. T.; Van Hoesen, G. W.; Damasio, A. R. and Barnes, C. L. Alzheimer's disease: cell-specific pathology isolates the hippocampal formation. *Science*. **1984**, *225*, 1168-1170.

8. Glennie, J. (1997) The efficacy of tacrine and the measurement of outcomes in Alzheimer's disease. Ottawa: Canadian Coordinating Office for Health Technology Assessment (CCOHTA).

9 .Etienne, P.; Dastoor, D.; Gauthier, S.; Ludwick, R. and Collier, B. Alzheimer disease: lack of effect of lecithin treatment for three months. *Neurology*. **1981**, *31*, 1552-1554.

10. Christie, J. E.; Shering, A.; Ferguson, J. and Glen, A. I. Physostigmine and arecoline: effects of intravenous infusions in Alzheimer presenile dementia. *Br. J. of Psychiatry*. **1981**, *138*, 46-50.

11. Mohr, E.; Mendis, T.; Rusk, I. N. and Grimes, J. D. Neurotransmitter replacement therapy in Alzheimer's disease. *J. Psychiatry and Neurosci.* **1994**, *19*, 17-23.

12. Groner, E.; Ashani, Y.; Schorer-Apelbaum, D.; Sterling, J.; Herzig, Y. and Weinstock, M. The kinetics of inhibition of human acetylcholinesterase and butyrylcholinesterase by two series of novel carbamates. *Mol. Pharmacol.* **2007**, *71*, 1610-1617.

13. Arendt, T.; Bruckner, M. T.; Lange, M. and Bigl, V. Changes in acetylcholinesterase and butyrylcholinesterase in Alzheimer's disease resemble embryonic development. *Neurochem. Int.* **1992**, *21*, 381-396.

14. Alzheimer Society of Canada. Living with dementia: drugs approved for Alzheimer's disease. http://www.alzheimer.ca/en/Living-with-dementia/Treatment-options/Drugs-approved-for-Alzheimers-disease (accessed April 17, 2015).

15. Atri, A.; Molinuevo, J. L.; Lemming, O.; Wirth, Y.; Pulte, I. and Wilkinson, D. Memantine in patients with Alzheimer's disease receiving donepezil: new analyses of efficacy and safety for combination therapy. *Alzheimers Res. Ther*. **2013**, *5*, 6.

16. Hardy, J. A. and Higgins, G. A. Alzheimer's disease: the amyloid cascade hypothesis. *Science*. **1992**, *256*, 184-185.

17. Verdile, G.; Fuller, S.; Atwood, C. S.; Laws, S. M.; Gandy, S. E. and Martins, R. N. The role of beta amyloid in Alzheimer's disease: still a cause of everything or the only one who got caught? *Pharmacol. Res.* **2004***, 50,* 397-409.

18. Sommer, B. Alzheimer's disease and the amyloid cascade hypothesis: ten years on. *Curr. Opin. Pharmacol*. **2002**, *2*, 87-92.

19. Hartley, D. M.; Walsh, D. M.; Ye, C. P.; Diehl, T.; Vasquez, S.; Vassilev, P. A.; Teplow, D. B. and Selkoe, D. J. Protofibrillar intermediates of amyloid β-protein induce acute electrophysiological changes and progressive neurotoxicity in cortical neurons. *J. Neurosci.* **1991**, *19*, 8876-8884.

20. Inestrosa, N. C.; Alvarez, A.; Pérez, C. A.; Moreno, R. D.; Vicente, M.; Linker, C.; Casanueva, O. I.; Soto, C. and Garrido, J. Acetylcholinesterase accelerates assembly of amyloid-β-peptides in Alzheimer's fibrils: possible role of the peripheral site of the enzyme. *Neuron*. **1996**, *16*, 881-891.

21. Johnson, G. and Moore, S. W. The peripheral anionic site of acetylcholinesterase: structure, functions and potential role in rational drug design. *Curr. Pharm. Des.* **2006**, *12,* 217-225.

22. Reyes, A. E.; Chacón, M. A.; Dinamarca, M. C.; Cerpa, W.; Morgan, C. and Inestrosa, N. C. Acetylcholinesterase-Aβ complexes are more toxic than Aβ fibrils in rat hippocampus. *Am. J. Pathol.* **2004***, 164*, 2163-2174.

23 . Castro, A. and Martinez, A. Targeting beta-amyloid pathogenesis through acetylcholinesterase inhibitors. *Curr. Pharm. Des.* **2006**, *12*, 4377-4387.

24 .Watkins, P. B.; Zimmerman, H. J.; Knapp, M. J.; Gracon, S. I. and Lewis, K. W. Hepatotoxic effects of tacrine administration in patients with Alzheimer's disease. *JAMA*. **1994**, *271*, 992-998.

25. Park, B. K.; Madden, S.; Spaldin, V.; Woolf, T. F. and Pool, W. F. Tacrine transaminitis: potential mechanisms. *Alzheimer Dis. Assoc. Disord.* **1994**, 8.

26 . James, L. P.; Mayeux, P. R. and Hinson, J. A. Acetaminophen-induced hepatotoxicity. *Drug Metab. Dispos*. **2003**, *31*, 1499-1506.

27. Guengerich, F. P. Cytochrome p450 and chemical toxicology. *Chem. Res. Tox.* **2008**, *21*, 70-83.

28. Faber, M. S.; Jetter, A. and Fuhr, U. (2005) Assessment of CYP1A2 activity in clinical practice: why, how, and when? *Basic Clin. Pharmacol. Toxicol.* **2005**, *97*, 125-134.

29. De Rienzo, F.; Fanelli, F.; Menziani, M. C. and De Benedetti, P. G. Theoretical investigation of substrate specificity for cytochromes P450 IA2, P450 IID6 and P450 IIIA4. *J. Comput Aided Mol. Des.* **2000**, *14*, 93-116.

30. Itoh, T.; Takemura, H.; Shimoi, K. and Yamamoto, K. A 3D model of CYP1B1 explains the dominant 4-hydroxylation of estradiol. *J. Chem. Inf. Model*. **2010**, *50*, 1173-1178.

31. Sansen, S.; Yano, J. K.; Reynald, R. L.; Schoch, G. A.; Griffin, K. J.; Stout, C. D. and Johnson, E. F. Adaptations for the oxidation of polycyclic aromatic hydrocarbons exhibited by the structure of human P450 1A2. *J. Biol. Chem.* **2007**, *282*, 14348-14355.

32. Parikh, A.; Josephy, P. D. and Guengerich, F. P. Selection and characterization of human cytochrome P450 1A2 mutants with altered catalytic properties. *Biochemistry*. **1999**, *38*, 5283-5289.

33. Szymanski, P.; Skibinski, R.; Inglot, T.; Bajda, M. I.; Jonczyk, J.; Malawska, B. and Mikiciuk-Olasik, E. New tacrine analogs as acetylcholinesterase inhibitors – theoretical study with chemometric analysis. *Molecules*. **2013**, *18*, 2878-2894.

34. Chen, Y.; Sun, J.; Fang, L.; Liu, M.; Peng, S.; Liao, H.; Lehmann, J. and Zhang, Y. Tacrine-ferulic acid-nitric oxide (NO) donor trihybrids as potent, multifunctional acetyl- and butyrylcholinesterase inhibitors. *J. Med. Chem.* **2012**, *55*, 4309-4321.

35. Bolognesi, M. L.; Cavalli, A.; Valgimigli, L.; Bartolini, M.; Rosini, M.; Andrisano, V.; Recanatini, M. and Melchiorre, C. Multi-target-directed drug design strategy: from a dual binding site acetylcholinesterase inhibitor to a trifunctional compound against Alzheimer's disease. *J. Med. Chem.* **2007**, *50*, 6446-6449.

36. Rosini, M.; Simoni, E.; Bartolini, M.; Cavalli, A.; Ceccarini, L.; Pascu, N.; McClymont, D. W.; Tarozzi, A.; Bolognesis, M. L.; Minarini, A.; Tumiatti, V.; Andrisano, V.; Mellor, I. R. and Melchiorre, C. Inhibition of acetylcholinesterase, β-amyloid aggregation, and NMDA receptors in Alzheimer's disease: a promising direction for the multi-target-directed ligands gold rush. *J. Med. Chem.* **2008**, *51*, 4381-4384.

37. Osman, W. Design, synthesis, and evaluation of tacrine-based derivatives: potential agents to treat Alzheimer's disease. **2013**. M. Sc. Thesis. University of Waterloo: Canada.

38. Marambaud, P.; Zhao, H. and Davies, P. Resveratrol promotes clearance of Alzheimer's disease amyloid-β peptides. *J. Biol. Chem.* **2005**, *280*, 37377-37382.

39. Wang, Y.-J.; Zhou, H.-D. and Zhou, X.-F. Clearance of amyloid-beta in Alzheimer's disease: progress, problems and perspectives. *Drug Discov. Today*. **2006**, *11*, 931-938.

40. Bartolini, M.; Bertucci, C.; Cavrini, V. and Andrisano, V. Amyloid aggregation induced by human acetylcholinesterase: inhibition studies. *Biochem. Pharmacol*. **2003**, *65*, 407-416.

41. Matharu, B.; Gibson, G.; Parsons, R.; Huckerby, T. N.; Moore, S. A.; Cooper, L. J.; Millichamp, R.; Allsop, D. and Austen, B. Galantamine inhibits β-amyloid aggregation and cytotoxicity. *J. Neurol. Sci*. **2009**, *280*, 49-58.

42. Manji, H. K. and DeSouza, E. B. CNS drug discovery and development: when will we rescue Tantalus? *Neuropsychopharmacol. Rev*. **2008**, *2*, 1-4.

43. Kaitin, K. I. and Milne, C. P. A dearth of new meds: drugs to treat neuropsychiatric disorders have become too risky for Big Pharma. *Sci. Am*. **2011**, *305*, 16.

44. Riordan H. J. and Cutler, N. R. The death of CNS drug development: overstatement or omen? *J. Clin. Studies*. **2011**, *3*, 12-15.

45. Hansch, C.; Steward, A. R.; Anderson, S. M. and Bentley, D. The parabolic dependence of drug action upon lipophilic character as revealed by a study of hypnotics. *J. Med. Chem.* **1967**, *11*, 1-11.

46. Arnott, J. A.; Kumar, R. and Lobo Planey, S. Lipophilicity indices for drug development. *J. Appl. Biopharm. Pharmacokin.* **2013**, *1*, 31-36.

47. Onizuka, S.; Yonaha, T. and Tsuneyoshi, I. Local anesthetics with high lipophilicity are toxic, while local anesthetics with low pka induce more apoptosis in human leukemia cells. *J. Anesth. Clin. Res*. **2011**, *2*, 116.

48. Nava-Ocampa, A. A. and Bello-Ramírez, A. M. Lipophilicity affects the pharmacokinetics and toxicity of local anaesthetic agents administered by caudal block. *Clin. Exp. Pharmacol. Physiol.* **2004**, *31*, 116-118.

49. Hann, M. M. and Keserü, G. M. Finding the sweet spot: the role of nature and nurture in medicinal chemistry. *Nat. Rev. Drug Discov.* **2012**, *11*, 355-365.

50. Lipinski, C. A.; Lombaro, F.; Dominy, B. W. and Feeney, P. J. Experimental and computational approaches to estimate solubility and permeability in drug discovery and development settings. *Adv. Drug Deliv. Rev.* **1997**, *23*, 3-25.

51. Lipinski C. A. Drew University Medicinal Chemistry Special Topics Course 1999.

52. Veber, D. F.; Johnson, S. T.; Cheng, H.-Y.; Smith, B. R.; Ward, K. W. and Kopple, K. D. (2002) Molecular properties that influence the oral bioavailability of drug candidates. *J. Med. Chem.* **2002**, *45*, 2615-2623.

53. Abbott, N. J.; Patabendige, A. A. K.; Dolman, D. E., M.; Yusof, S. R. and Begley, D. J. Structure and function of the blood-brain barrier. *Neurobiol. Dis.* **2010**, *37*, 13-25.

54. Aller, S. G.; Yu, J.; Ward, A.; Weng, Y.; Chittaboina, S.; Zhou, R.; Harrell, P. M.; Trinh, Y. T.; Zhang, W.; Urbatsch, I. L. and Chang, G. Molecular basis for poly-specific drug binding. *Science*. **2009**, *323*, 1718-1722.

55. Liu, M.; Hou, T.; Feng, Z. and Li, Y. The flexibility of P-glycoprotein for its poly-specific drug binding from molecular dynamics simulations. *J. Biomol. Struct. Dyn.* **2012**, *31*, 612-629.

56. Sauna, Z. E. and Ambudkar, S.V. Characterization of the catalytic cycle of ATP hydrolysis by human P-glycoprotein: the two ATP hydrolysis events in a single catalytic cycle are kinetically similar but affect different functional outcomes. *J. Biol. Chem.* **2001**, *276*, 11653–11661.

57. Ambudkar, S. V.; Kim, I.-W. and Sauna, Z. E. The power of the pump: mechanisms of action of P-glycoprotein (ABCB1). *Eur. J. Pharm. Sci.* **2006**, *27*, 392-400.

58. Cummins, C. L.; Jacobsen, W. and Benet, L. Z. Unmasking the dynamic interplay between intestinal P-glycoprotein and CYP3A4. *J. Pharmacol. Exp. Ther.* **2002**, *300*, 1036-1045.

59. Breedveld, P.; Beijnen, J. H. and Schellens, J. H. M. Use of P-glycoprotein and BCRP inhibitors to improve oral bioavailability and CNS penetration of anticancer drugs. *Trends Pharmacol. Sci.* **2006**, *27*, 17-24.

60. Terkeltaub, R. A.; Furst, D. E.; DiGiacinto, J. L.; Kook, K. A. and Davis, M. W. Evidence-based colchicine dose-reduction algorithm to predict and prevent colchicine toxicity in the presence of cytochrome P450 3A4/P-glycoprotein inhibitors. *Arthritis Rheumatol.* **2011**, *63*, 2226-2237.

61. Jones, H. M. and Rowland-Yeo, K. Basic concepts in physiologically based pharmacokinetic modeling in drug discovery and development. *CPT Pharmacometrics Syst. Pharmacol.* **2013**, *2*, 63-74.

62. Gerlowski, L. E. and Jain, R. K. Physiologically based pharmacokinetic modeling: principles and applications. *J. Pharm. Sci.* **1983**, *72*, 1103-1127.

63. Westerhout, J.; Ploeger, B.; Smeets, H.; Danhof, M. and Delange, E. C. M. Physiologically based pharmacokinetic modeling to investigate regional brain distribution kinetics in rats. *AAPS J.* **2012**, *15*, 543-553.

64. Ball, K.; Bouzom, F.; Walther, B.; Declèves, X. Development of a physiologically based pharmacokinetic model for the rat central nervous system and determination of an *in vitro-in vivo* scaling methodology for the blood-brain barrier permeability of two transporter substrates, morphine and oxycodone. *J. Pharm. Sci.* **2012**, *101*, 4277-4292.

65. Tunblad, K.; Hammarlund-Udenaes, M. and Jonsson, E. N. An integrated model for the analysis of pharmacokinetic data from microdialysis experiments. *Pharm. Res.* **2004**, *21*, 1698-1707.

66 . Ball, K.; Bouzom, F.; Scherrmann, J.-M.; Walther, B. and Declèves, X. Physiologically based pharmacokinetic modeling of drug penetration across the blood-brain barrier – towards a mechanistic IVIVE-based approach. *AAPS J.* **2013**, *15*, 913-932.

67. Yu, Q.; Zhu, X.; Holloway, H. W.; Whittaker, N. F.; Brossi, A. and Greig, N. H. Anticholinesterase activity of compounds related to geneserine tautomers. *N*-oxides and 1,2-oxazines. *J. Med. Chem.* **2002**, *45*, 3684-3691.

68. Feng, B.; Mills, J. B.; Davidson, R. E.; Mireles, R. J.; Janiszewski, J. S.; Troutman, M. D. and de Morais, S. M. *In vitro* P-glycoprotein assays to predict the *in vivo* interactions of P-glycoprotein with drugs in the central nervous system. *Drug Metab. Dispos.* **2008**, *36*, 268-275.

69. Tiberghien, F. and Loor, F. Ranking of P-glycoprotein substrates and inhibitors by a calcein-AM fluorometry screening assay. *Anticancer Drugs*. **1996**, *7*, 568-578.

70. Ramachandra, M.; Ambudkar, S. V.; Chen, D.; Hrycyna, C. A.; Dey, S.; Gottesman M. M. and Pastan, I. Human P-glycoprotein exhibits reduced affinity for substrates during a catalytic transition state. *Biochemistry*. **1998**, *37*, 5010-5019.

71. Polli, J. W.; Wring, S. A.; Humphreys, J. E.; Huang, L.; Morgan, J. B.; Webster, L. O. and Serabhit-Singh, C. S. Rational use of *in vitro* P-glycoprotein assays in drug discovery. *J. Pharmacol. Exp. Ther.* **2001**, *299*, 620-628.

72. Fowler, B. A.; Haach, M. L.; Squibb, K. S. and Hayes A. W. Organelles as Tools in Toxicology. In: Hayes, A. W., ed. Principles and Methods of Toxicology. New York, NY: Informa; 2008: p. 1939.

73. James, G. T. Inactivation of the protease inhibitor phenylmethylsulfonyl fluoride in buffers. *Anal. Biochem.* **1978**, *86*, 574-579.

74. Bradford, M. M. A rapid and sensitive method for the quantitation of microgram quantities of protein utilizing the principle of protein-dye binding. *Anal. Biochem*. **1976**, *72*, 248-254.

75. Compton, S. J. and Jones, C. G. Mechanism of dye response and interference in the Bradford protein assay. *Anal. Biochemistry*. **1985** *151*, 369-374.

76. Pandey, A. M. and Flück, C. E. NADPH P450 oxidoreductase: structure, function, and pathology of diseases. *Pharmacol. Ther.* **2013**, *138*, 229-254.

77. Yim, S. K.; Yun, S. J. and Yun, C. H. A continuous spectrophotometric assay for NADPH-cytochrome P450 reductase activity using 1,1-diphenyl-2-picrylhydrazyl. *J. Biochem. Mol. Biol.* **2004**, *37*, 629-633.

78. Telting-Diaz and Lunte. Distribution of tacrine across the blood-brain barrier in awake, freely moving rats using *in vivo* microdialysis sampling. *Pharm. Res.* **1993**, *10*, 44-48.

79. MacKichan, J. J. (1992) Influence of protein binding and use of unbound (free) drug concentrations. In: *Applied Pharmacokinetics & Pharmacodynamics: Principles of Therapeutic Drug Monitoring*; Burton, M. E., Ed.; Lippincott Williams & Wilkins, p 100.

80. Laine, K.; Palovaara, S.; Tapanainen, P. and Manninen, P. Plasma tacrine concentrations are significantly increased by concomitant hormone replacement therapy. *Clin. Pharmacol. Ther.* **1999**, *66*, 602-608.

81. Sung, J.-H.; Yu, K.-H.; Park, J.-S.; Tsuruo, T.; Kim, D.-D.; Shim, C.-K. and Chung, S.-J. Saturable distribution of tacrine into the striatal extracellular fluid of the rat: evidence of involvement of multiple organic cation transporters in the transport. *Drug Metab. Dispos.* **2005**, *33*, 440-448.

82. Grieg, N. H.; Kamal, M. A.; Jabir, N. R.; Tabrez, S.; Nasim, F. H.; Abuzenadah, A. M. and Aliev, G. (2014) Specific cholinesterase inhibitors: a potential tool to assist in management of Alzheimer disease. In: *Drug Design and Discovery in Alzheimer's Disease*; Rahman, A. and Choudhary, M. I., Eds.; Elsevier, p 379.

83. Taylor, R. D.; Jewsbury, P. J. and Essex, J. W. A review of protein-small molecule docking methods. *J. Comput. Aided Mol. Des.* **2002**, *16*, 151-166.

84. Halperin, I.; Ma, B.; Wolfson, H. and Nussinov, R. Principles of docking: an overview of search algorithms and a guide to scoring functions. *Proteins*. **2002**, *47*, 409-443.

85. Locuson, C. W.; Hutzler, J. M. and Tracy, T. S. Visible spectra of type II cytochrome P450-drug complexes: evidence that "incomplete" heme coordination in common. *Drug Metab. Dispos.* **2007**, *35*, 614-622.

86. Jones, J. P.; Joswig-Jones, C. A.; Hebner, M.; Chu, Y. and Koop, D. R. (2011) The effects of nitrogen-heme-iron coordination on substrate affinities for cytochrome P450 2E1. *Chemico-Biological Interactions*, 192, 50-56.

87. Strickler, M.; Goldstein, B. M.; Maxfield, K.; Shireman, L.; Kim, G.; Matteson, D. S. and Jones, J. P. Crystallographic studies on the complex behaviour of nicotine binding P450cam (CYP101). *Biochemistry*. **2003**, *42*, 11943-11950.

88. Sharom, F. J. The P-glycoprotein multidrug transporter. *Essays Biochem.* **2011**, *50*, 161-178.

89. Loo, T. W. and Clarke, D. M. Identification of residues in the drug-binding site of human P-glycoprotein using a thiol-reactive substrate. *J. Biol. Chem.* **1997**, *272*, 31945-31948.

90. Loo, T. W. and Clarke, D. M. Drug rescue distinguishes between different structural models of human P-glycoprotein. *Biochemistry*. **2013**, *52*, 7167-7169.

91. Yasuda, K.; Lan, L.-B.; Sanglard, D.; Furuya, K.; Schuetz, J. D. and Schuetz, E. G. Interaction of cytochrome P450 3A inhibitors with P-glycoprotein. *J. Pharmacol. Exp. Ther.* **2002**, *303*, 323-332.

92 . McEneny-King, A.; Edginton, A. N. and Rao, P. P. N. Investigating the binding interactions of the anti-Alzheimer's drug donepezil with CYP3A4 and P-gp. *Bioorg. Med. Chem. Lett.* **2015**, *25*, 297-301.

93. Tiseo, P. J.; Perdomo, C. A. and Friedhoff, L. T. Metabolism and elimination of 14C-donepezil in healthy volunteers: a single-dose study. *Br. J. Clin. Pharmacol.* **1998**, *46*, 19-24.

94. Matsui, K.; Mishima, M.; Nagai, Y.; Yuzuriha, T. and Yoshimura, T. Absorption, distribution, metabolism, and excretion of donepezil (Aricept) after a single oral administration to rat. *Drug Metab. Dispos.* **1999**, *27*, 1406-1414.

95. Wager, T. T.; Chandrasekaran, R. Y.; Hou, X.; Troutman, M. D.; Verhoest, P. R.; Villalobos, A. and Will, Y. Defining desirable central nervous system drug space through the alignment of molecular properties, *in vitro* ADME, and safety attributes. *ACS Chem. Neurosci.* **2010**, *1*, 420-434.

96. Summerfield, S. G.; Read, K.; Begley, D. J.; Obradovic, T.; Hidalgo, I. J.; Coggon, S.; Lewis, A. V.; Porter, R. D. and Jeffrey, P. Central nervous system drug disposition: the relationship between in situ brain permeability and brain free fraction. *J. Pharamcol. Exp. Ther.* **2007**, *322*, 201-213.

97. Ishiwata, K.; Kawamura, K.; Yanai, K. and Hendrikse, N. H. *In vivo* evaluation of P-glycoprotein modulation of 8 PET radioligands used clinically. *J. Nucl. Med.* **2007**, *48*, 81-87.

98. Bentham, L. C. The use of *in vitro* unbound drug fraction and permeability in predicting central nervous system drug penetration. **2010**. PhD Thesis. University of Manchester: United Kingdom.

99. Clinical Pharmacology and Biopharmaceutics Review, Center for Drug Evaluation and Research, Application Number 022568, US FDA 2010 (http://www.accessdata.fda.gov/drugsatfda_docs/nda/2010/022568orig1s000clinpharmr.pdf).

100. Benet, L. Z.; Cummins, C. L. and Wu, C. Y. Unmasking the dynamic interplay between efflux transporters and metabolic enzymes. *Int. J. Pharm.* **2004**, *277*, 3-9.

101. Baxter, J. G.; Brass, C.; Schentag, J. J. and Slaughter, R. L. Pharmacokinetics of ketoconazole administered intravenously to dogs and orally as tablet and solution to humans and dogs. *J. Pharm. Sci.* **2006**, *75*, 443-447.

102. Gunaydin, H.; Weiss, M. M. and Sun, Y. De novo prediction of P-glycoprotein-mediated efflux liability for druglike compounds. *ACS Med. Chem. Lett.* **2012**, *4*, 108-112.

103. Mahar Doan, K. M.; Humphreys, J. E.; Webster, L. O.; Wring, S. AR.; Shampine, L. J.; Serabjit-Singh, C. J.; Adkison, K. K. and Polli, J. W. Passive permeability and P-glycoprotein-mediated efflux differentiate central nervous systems (CNS) and non-CNS marketed drugs. *J. Pharm. Exp. Ther.* **2002**, *303*, 1029-1037.

104. Liu, M.; Hou, T.; Feng, Z. and Li, Y. The flexibility of P-glycoprotein for its poly-specific drug binding from molecular dynamics simulations. *J. Biomol. Struc. Dyn.* **2013**, *31*, 612-629.

105. Ferreira, R. J.; Ferreira, M.-J. U. and dos Santos, D. J. V. A. Insights on P-glycoprotein's efflux mechanism obtained by molecular dynamics simulations. *J. Chem. Theory Comput.* **2012**, *8*, 1853-1864.

106. Lehmann, J. M.; McKee, D. D.; Watson, M. A.; Willson, T. M.; Moore, J. T. and Kliewer, S. A. The human orphan nuclear receptor PXR is activated by compounds that regulate *CYP3A4* gene expression and cause drug interactions. *J. Clin. Invest.* **1998**, *102*, 1016-1023.

107. Fahmi, O. A.; Hurst, S.; Plowchalk, D.; Cook, J.; Guo, F.; Youdim,K.; Dickins, M.; Phipps, A.; Darekar, A.; Hyland, R. and Obach, R. S. Comparison of different algorithms for predicting clinical drug-drug interactions, based on the use of CYP3A4 *in vitro* data: predictions of compounds as precipitants of interaction. *Drug Metab. Dispos.* **2009**, *37*, 1658-1666.

108. Ekroos, M. and Sjögren, T. Structural basis for ligand promiscuity in cytochrome P450 3A4. *Proc. Natl. Acad. Sci.* **2006**, *103*, 13682-13687.

109. Houston, J. B. Utility of *in vitro* drug metabolism data in predicting *in vivo* metabolic clearance. *Biochem. Pharmacol.* **1994**, *47*, 1469-1479.

110. Mohutsky, M. A.; Chien, J. Y.; Ring, B. J. and Wrighton, S. A. Predictions of the *in vivo* clearance of drugs from rate of loss using human liver microsomes for phase I and phase II biotransformations. *Pharm Res.* **2006**, *23*, 654-662.

111. Obach, R. S. and Reed Hagen, A. E. Measurement of Michaelis constants for cytochrome P450-mediated biotransformation reactions using a substrate depletion approach. *Drug Metab. Dispos.* **2002**, *23*, 654-662.

112. Nath, A. and Atkins, W. M. A theoretical validation of the substrate depletion approach to determining kinetic parameters. *Drug Metab. Dispos.* **2006***, 34*, 1433-1435.

113. Flanagan, R. J.; Taylor, A.; Watson, I. D. and Whelpton, R. *Fundamentals of Analytical Toxicology*; John Wiley & Sons: West Sussex, 2007.

114. Ekblom, M.; Hammarlund-Udenaes, M.; Lundqvist, T. and Sjöberg, P. Potential use of microdialysis in pharmacokinetics: a protein binding study. *Pharm. Res.* **1992**, *9*, 155-158.

115. Sarre, S.; Van Belle, K.; Smolders, I.; Krieken, G. and Michotte, Y. The use of microdialysis for the determination of plasma protein binding of drugs. *J. Pharm. Biomed. Anal.* **1992**, *10*, 735-739.

116. Le Quellec, A.; Dupin, S.; Tufenkji, A. E.; Genissel, P. and Houin, G. Microdialysis: an alternative for *in vitro* and *in vivo* protein binding studies. *Pharm. Res.* **1994**, *11*, 835-838.

117. Carlile, D. J.; Hakooz, N.; Bayliss, M. K. and Houston, J. B. Microsomal prediction of *in vivo* clearance of CYP2C9 substrates in humans. *Br. J. Clin. Pharmacol.* **1999**, *47*, 625-635.

118. Obach, R. S. Nonspecific binding to microsomes: impact on scale-up of *in vitro* intrinsic clearance to hepatic clearance as assessed through examination of warfarin, imipramine, and propranolol. *Drug Metab. Dispos.* **1997**, *25*, 1359-1369.

119. Austin, R. P.; Barton, P.; Cockroft, S. L.; Wenlock, M. C. and Riley, R. J. The influence of nonspecific microsomal binding on apparent intrinsic clearance, and its prediction from physicochemical properties. *Drug Metab. Dispos.* **2002**, *30*, 1497-1503.

120. Peters, S. A. *Physiologically-Based Pharmacokinetic (PBPK) Modeling and Simulations: Principles, Methods, and Applications in the Pharmaceutical Industry*; John Wiley & Sons, Hoboken, 2012.

121. Leach, K. G.; Karran, S. J.; Wisbey, M. L. and Blumgart, L. H. *In vivo* assessment of liver size in the rat. *J. Nucl. Med.* **1975**, *16*, 380-385.

122. Ito, K. and Houston, J. B. Prediction of human drug clearance from *in vitro* and preclinical data using physiologically based and empirical approaches. *Pharm. Res.* **2005**, *22*, 103-112.

123. Rats! *Nat. Methods.* **2010**, *7*, 413.

124. Goutianos, G.; Tzioura, A.; Kyparos, A.; Paschalis, V.; Margaritelis, N. V.; Veskoukis, A. S.; Zafeiridis, A.; Dipla, K.; Nikolaidis, M. G. and Vrabas, I. S. The rat adequately reflects human responses to exercise in blood biochemical profile: a comparative study. *Physiol. Rep.* **2015**, *3*, e12293.

125. Kuempel, E. D.; Smith, R. J.; Dankovic, D. A.; Bailer, A. J. and Stayner, L. T. Concordance of rat- and human-based risk estimation for particle-related lung cancer. *Ann. Occup. Hyg.* **2002**, *46*, 62-66.

126. Cohen, R. M.; Rezai-Zadeh, K.; Weitz, T. M.; Rentsendorj, A.; Gate, D.; Spivak, I.; Bholat, Y.; Vasilevko, V.; Glabe, C. G.; Breunig, J. J.; Rakic, P.; Davtyan, H.; Agadjanyan, M. G.; Kepe, V.; Barrio, J. R.; Bannykh, S.; Szekely, C. A.; Pechnick, R. N. and Town, T. A transgenic Alzheimer rat with plaques, tau pathology, behavioural impairment, oligomeric AB, and frank neuronal loss. *J. Neurosci.* **2013**, *33*, 6245-6256.

127. Lecanu, L. and Papadopoulos, V. Modeling Alzheimer's disease with non-transgenic rat models. *Alzheimers. Res. Ther.* **2013**, *5*, 17.

128. Do Carmo, S. and Cuello, A. C. Modeling Alzheimer's disease in transgenic rats. *Mol. Neurodegener.* **2013**, *8*, 37.

129. Goh, C. W.; Aw, C. C.; Lee, J. H.; Chen, C. P. and Browne, E. R. Pharmacokinetic and pharmacodynamics properties of cholinesterase inhibitors donepezil, tacrine, and galantamine in aged and young Lister hooded rats. *Drug Metab. Dispos.* **2010**, *39*, 402-411.

130. Perrin, D. D. *Dissociation Constants of Organic Bases in Aqueous Solution*; Butterworths: London, 1965.

131. Hediger, M. A.; Romero, M. F.; Peng, J. B.; Rolfs, A.; Takanaga, H. and Bruford, E. A. The ABCs of solute carriers: physiological, pathological and therapeutic implications of human membrane transporter proteins. *Pflügers Arch.* **2004**, *447*, 465-468.

132. Rodgers, T. and Rowland, M. Physiologically based pharmacokinetic modelling 2: predicting the tissue distribution of acids, very weak bases, neutrals and zwiterions. *J. Pharm. Sci.* **2006**, *95*, 1238-1257..

133. Hendrickx, R.; Johansson, J. G.; Lohmann, C.; Jenvert, R.-M.; Blomgren, A.; Börjesson, L. and Gustavsson, L. Identification of novel susbtrates and structure-activity relationship of cellular uptake mediated by human organic cation transporters 1 and 2. *J. Med. Chem.* **2013**, *56*, 7232-7242.

134. Xu, Y.; Liu, X.; Li, S.; Zhou, N.; Gong, L.; Luo, C.; Luo, X.; Zheng, M.; Jiang, H. and Chen, K. Combinatorial pharmacophore modeling of organic cation transporter 2 (OCT2) inhibitors: insights into multiple inhibitor mechanisms. *Mol. Pharmaceutics.* **2013**, *10*, 4611-4619.

135. Suhre, W. M.; Ekins, S.; Chang, C.; Swaan, P. W. and Wright, S. H. Molecular determinants of substrate/inhibitor binding to the human and rabbit renal organic cation transporters hOCT2 and rbOCT2. *Mol. Pharmacol.* **2005**, *67*, 1067-1077.